On the formation and spreading of thermohaline intrusions in the Arctic Ocean

Bert Rudels[1] and Dagmar Hainbucher[2]

[1]Finnish Meteorological Institute, Erik Palmenin aukio 1, FI-00560 Helsinki, Finland
bert.rudels@fmi.fi

[2]Institute of Oceanography, University of Hamburg, Bundesstraße 53, D-20146 Hamburg, Germany
Dagmar.Hainbucher@uni-hamburg.de

Abstract

The Arctic Ocean is a high latitude, ice covered ocean in its upper part strongly stratified in salinity and the warm Atlantic water entering through Fram Strait and the Barents Sea is isolated from surface driven mechanical and thermohaline forcing. This allows other mixing processes such as double-diffusive convection to become important and it has been argued that interleaving, driven by double-diffusive convection, may increase the exchange of Atlantic water between the boundary current and the interior of the basins. Although intrusions are present practically everywhere in the Arctic Ocean their formation has been more difficult to observe. Here it is postulated that intrusions are created almost instantaneously at narrow fronts, where waters with different mixing histories come into contact, especially at the strongest front in the Arctic Ocean, formed at the Kara Sea slope as the two Atlantic inflow branches again meet. A conceptual model is used to describe the formation of intrusions. Two water masses separated by a narrow front are assumed to have the same vertical density, but different salinity and temperature stratifications. The thickness of the intrusions is estimated by requiring that the temperatures are equilibrated in vertical boundary layers between the water masses. This implies upward motion on the cold side, downward on the warm side. The motions are antisymmetric across the front and stop when the waters have attained the same temperature. The water on the cold side is then less dense than that on the warm side and the waters in the boundary layer start to interleave, opening paths across the front for the main water masses. This gives the maximum vertical displacement, and it is unlikely that it is attained before the boundary layers either go unstable or become affected by external disturbances. The double-diffusive transports across the created diffusive and salt finger interfaces homogenize and change the density of the intrusions, driving the cross-frontal spreading. The situation when both heat and salt are initially stably stratified is examined in detail. If the stability at the interfaces separating the intrusions is weak, the transport across the diffusive interface dominates, cold intrusions rise and the salt finger interfaces might overturn. When the stability increases the transport across the salt finger interface becomes the largest and cold intrusions should sink. It is assumed that such change in slope does not take place. The intrusions then cease to expand, become fossil and are transported with the mean circulation around the Arctic Ocean.

Keywords: Arctic Ocean, Nansen Basin, double-diffusive convection, diffusive interfaces, salt fingers, thermohaline intrusions, interleaving

1   Introduction

The Arctic Ocean is a high latitude enclosed ocean subject to strong radiative and atmospheric forcing and large freshwater import from the rivers and from the atmosphere (Fig. 1). The stability in the upper layers is determined by the low salinity, which allows

the water to be cooled to freezing and sea ice to form during the polar night. In summer the ice reduces, by its high albedo, the absorbed solar radiation, keeping the temperature low. The ice cover and the strong stratification also diminish the effects of the mechanical and thermohaline forcing applied at the sea surface and make the deeper layers of the Arctic Ocean a low energy environment, where mixing processes, driven by other energy sources, may be important.
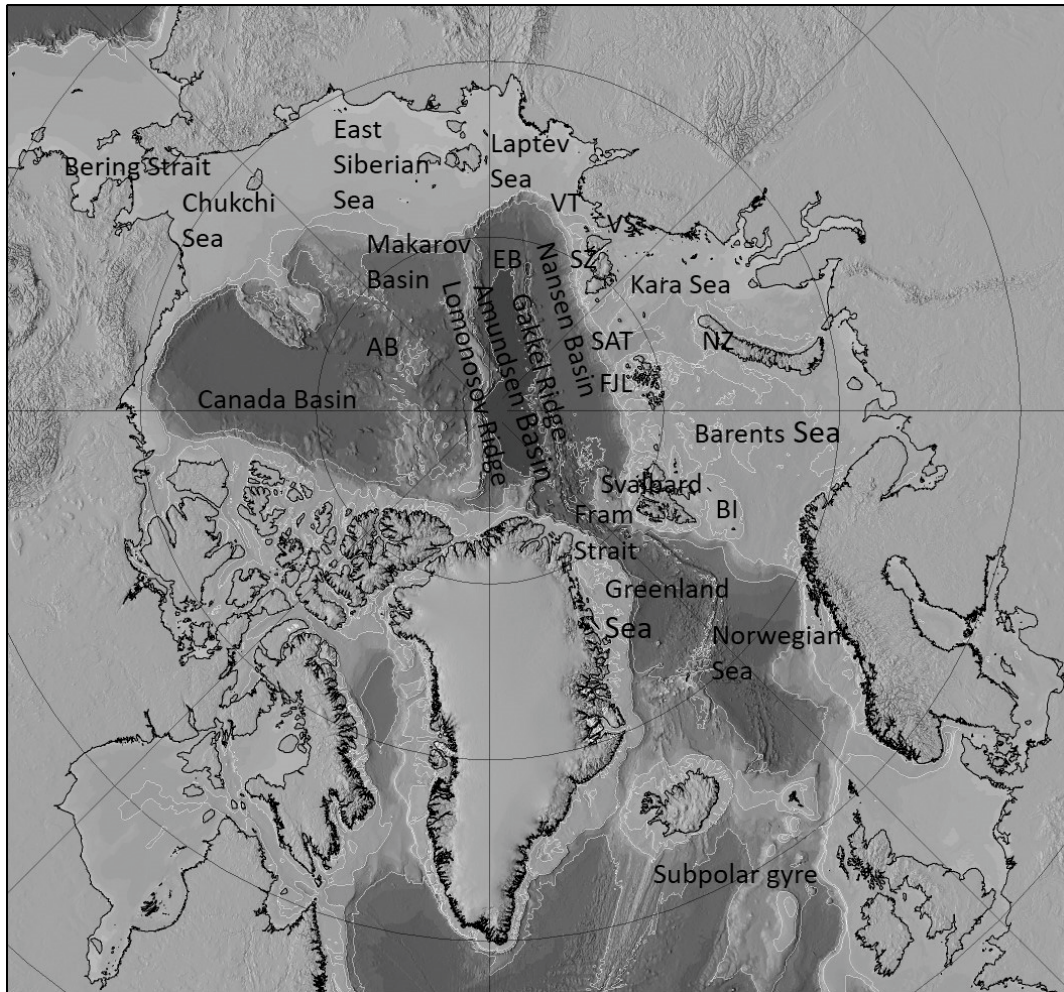

Fig. 1. Bathymetric map of the Arctic Mediterranean Sea. BI: Bear Island, FJL: Franz Josef Land, SAT: St Anna trough, SZ: Severnaya Zemlya, VS: Vilkitsky Strait, VT: Vilkitsky Trough, AB: Amerasian Basin, EB: Eurasian Basin. The map is supplied by Martin Jakobsson.

One such process is double-diffusive convection. Sea water is a two-component fluid and its density is determined by its temperature and its salinity. If, as in the Arctic Ocean, low salinity, cold water is located above warmer, more saline water, the density contribution due to heat is unstably stratified while that of salt is stably distributed. The opposite situation is when warm and saline water lies above colder and fresher water and salt is unstably stratified. If the unstable heat or salt distribution is removed, potential energy will be released, which could contribute to the mixing of the waters in the deep

ocean, away from the energy input applied at the sea surface. The mechanism that releases the stored potential energy is the more rapid molecular diffusion of heat than salt. In this study the possible importance of double diffusive processes, especially that of thermohaline intrusions in the Arctic Ocean, is addressed. Section 2 briefly presents the main characteristics of double-diffusive convection, and section 3 describes the thermohaline intrusions observed in the Arctic Ocean. In section 4 a conceptual approach for describing the formation of intrusions at a narrow front is introduced. Section 5 discusses the transports across the interfaces and section 6 relates the theoretical results to observation in the Arctic Ocean. Section 7 describes the spreading of the intrusions from the front to the interior of the basins, and a short summary is given in section 8. The approach concentrates on how thermohaline intrusions and interleaving are manifested in the ocean and what conclusion that might be drawn from their appearance.

Mechanically generated turbulence mixes heat and salt at the same rate, and to focus on and bring out the effects of the double-diffusive processes we assume that they act alone and supply all energy driving the mixing. The stirring that does take place is due to convection initiated by double-diffusive fluxes through the interfaces. The only exception is large-scale disturbances that might be required to create the first inversions initiating the double-diffusive convection (e.g. *Toole and Giorgi*, 1981)

2   Some characteristics of double-diffusive convection

When salt is unstably stratified a small vertical disturbance will bring warm water downward into a colder environment and cold water upward into a warmer environment. Heat diffuses out of the sinking water, making it more saline and denser than the ambient water and it will continue to sink. In similar manner the upward moving water is heated and since it is less saline it continues to rise. This type of convection is called salt finger convection and transports more salt than heat (in density units) downwards and thus releases potential energy (*Stern*, 1960; *Turner*, 1973; *Radko*, 2013). In the opposite situation with colder, less saline water overlying warmer, more saline water a warm, saline parcel displaced upward becomes cooled but retains its salinity and sinks back, but it may overshoot its original position and enter the warmer water below. Here it is heated still more and again rises and overshoots its original level. This type of instability is called overstability (*Veronis*, 1965, 1968). These oscillating motions, should they exist, have not been observed in the ocean but instead homogenous layers separated by thin gradients in temperature and salinity have been found in regions where temperature increases with depth. These structures, called diffusive staircases or diffusive interfaces, are sustained by the heat diffused through the sharp gradient regions, which makes the water immediately above warmer and below colder, leading to convection and homogenization of the layers and to transport of heat vertically upwards (*Turner*, 1965, 1973; *Linden and Shirtcliffe*, 1978; *Foldvik and Rudels*, 1996). More heat than salt is transported and the potential energy stored in the temperature distribution is released.

The strong stability in the Arctic Ocean makes the deeper layer, below 150 m to 200 m, dominated by the advection of water from lower latitudes. Especially the warm

Atlantic water that enters the Arctic Ocean through Fram Strait and over the Barents Sea remains beneath the low salinity upper layers and one question has been, if this heat, by vertical transfer through diffusive interfaces, could be made available to Arctic as a whole. This might be possible in the Nansen Basin, where the Atlantic water resides 100–150 m below the sea surface (e.g. *Polyakov* et al., 2019), but in the Canada Basin the Atlantic water is located deeper, below 200–250 m, and the staircases have smaller steps and layers and the estimated vertical double-diffusive heat transport is small (*Padman and Dillon*, 1987; *Timmermans et al.*, 2008). The diffusive interfaces are also separated from the sea surface by a temperature minimum, deriving from the Pacific winter inflow through Bering Strait. The temperature minimum prevents the heat from diffusing upragradient to the overlying warmer water, and it becomes trapped at the minimum.

The warm Atlantic water flows as a boundary current along the continental slopes around the Arctic Ocean and enters the different basins along bathymetric features. It has been proposed that double-diffusive processes could contribute to the spreading of heat from the slope to the interior of the basins by creating thermohaline intrusions (*Carmack et al.*, 1997; *Swift et al.*, 1997; *Walsh and Carmack*, 2003). The first theoretical description of thermohaline intrusions was given by *Stern* (1967), who considered a front where salt was unstably stratified (salt finger stratification) and that the horizontal temperature and salinity gradients across the front were density compensating. Stern related the vertical salt and heat transports through the salt finger interface by a salt finger flux ratio $Rf^F = F_{\alpha T}(F_{\beta S})^{-1} = \gamma$, with $\gamma < 1$. The heat expansion coefficient α is here taken as positive and β is the coefficient of salt contraction. He then found by linear stability analysis that disturbances bringing warm and saline water slightly upward within the front would grow and an interleaving of the two water masses could start.

Stern did not include friction in his model and the fastest growing disturbance was one with infinite wave number. *Toole and Giorgi* (1981) added friction and then obtained a fastest growing disturbance with finite layer thickness. The correspondence between observed and theoretically derived layer thicknesses has been one way of evaluating how well a model corresponds to observations. As the layers expand within the front diffusive interfaces start to develop between two salt finger interfaces and eventually the layers become separated by one salt finger interface and one diffusive interface. A warm intrusion has the salt finger interface below and a diffusive interface above and rises weakly within the front, while the situation is the opposite for a cold intrusion, which has a salt finger interface above and a diffusive interface below and sinks within the front.

This basic concept has been elaborated by several authors (*McDougall*, 1985a, b; *Ruddick and Hebert*, 1988; *Ruddick*, 1992; *May and Kelley*, 1997, 2002). Different approximations for the salt finger transport have been tried and the diffusive transports have been included. *Ruddick and Hebert* (1988) showed that a background diffusive stratification would also lead to interleaving but with the colder, less saline intrusions rising and the warm, saline intrusions sinking.

A second approach to explain oceanic interleaving is based on laboratory experiments first performed by *Ruddick and Turner* (1979). They studied a system with two stably stratified water masses, initially separated by a vertical wall. No horizontal density

gradients were present but the temperature and salinity were different at each side of the wall. Ruddick and Turner used salt as the fast diffusing substance (corresponding to heat) and sugar as the slower diffusing substance (corresponding to salt), and when the wall was removed the waters started to interleave. Ruddick and Turner assumed that the energy driving the water across the front was the potential energy released by downward transport of salt (sugar) through the created salt finger interfaces. They formulated a theoretical explanation for the observed thickness of the layers by invoking energy and stability arguments. The potential energy in the final state should be less than that of the initial state, and the density of the lower part of a layer should be less than the upper part of the layer below. Ruddick and Turner considered a layer as comprising both an upper warm intrusion and a lower cold intrusion moving in the opposite direction. Assuming an initial linear stable vertical density gradient gradρ and that the difference in salinity between the two water masses is βΔS the combined thickness H of the two intrusions becomes;

$$\frac{\beta \Delta S}{\rho_*^{-1} grad\rho}(1 - Rf^F) < H < \frac{3}{2}\frac{\beta \Delta S}{\rho_*^{-1} grad\rho}(1 - Rf^F) \tag{1}$$

A linear equation of state $\rho = \rho_*(1 - \alpha T + \beta S)$ is assumed, $Rf^F = F_{\alpha T}(F_{\beta S})^{-1}$ is the flux ratio and ρ_* the reference density. With other initial density profiles, the estimate will differ somewhat but have similar features. *Ruddick and Turner* (1979) assumed that the buoyancy transports through the salt finger interfaces dominate and given by the flux ratio Rf^F, while the corresponding transports through the diffusive interfaces would be small and could be ignored. Essentially, the scaling tells how far a parcel that crosses the front and loses its salinity excess by salt finger convection, taking the related heat flux into account, can rise in the stratification.

In the Ruddick and Turner experiments both properties were stably stratified and no infinitesimal instability could grow and generate intrusions. However, the two different water columns were close together, and any lateral disturbance (as when removing the wall) would allow the water columns to interleave and once this starts both diffusive and salt finger interfaces are created between the intrusions. The different transports of density anomalies across the two interfaces then change the density of the intrusions and drive them farther into the opposite water column.

The thickness is primarily determined by the salinity difference between the two water masses, which was supported by an experiment with one half stratified only in heat (salt) the other only in salt (sugar). The thickness of the intrusions then increased towards the bottom, where the largest βΔS and αΔT were found. Warm, saline intrusions appeared in the experiments to rise in agreement with the *Stern* (1967) model, but the layers were not straight but slightly wavy and at the fronts of the intrusions the warm intrusions might be sinking and the cold intrusions rising (*Ruddick and Turner* (1979, Fig. 3). In similar experiments made by *Holyer et al.* (1987) warm saline intrusions were sinking.

The vertical length-scale $\sim \beta \Delta S(\rho_*^{-1} grad\rho)^{-1}$ is similar to one obtained by *Thorpe et al.* (1969). They heated a tank with salinity stratified water at one vertical boundary. The water near the warm wall rose until it was stopped by the stratification and then moved

from the wall into the interior of the tank. The height of the wall was larger than the distance the parcels ascended and several layers were formed and return flows of cold water towards the wall were induced, feeding the water rising at the wall and establishing cellular circulations. In another experiment using a very narrow tank the opposite wall was cooled and closed circulation loops were established between the walls. As the warm water leaves the wall and enters the interior, it is gradually cooled by the overlying water and descends, while the water below moving towards the warm wall is heated and rises. This suggests that the interfaces between the cells are diffusive interfaces, while the interior of the circulation loops is unstably stratified in salinity and could sustain salt finger convection, although this was not discussed in the Thorpe et al. experiment.

One fundamental difference between intrusions created in the Ruddick and Turner experiment and the intrusions formed at a wide front with horizontally density compensating gradients is their time evolution. When horizontal gradients are present the temperature and salinity steps between the intrusive layers, as seen in the temperature and salinity profiles and in the TS curves, grow as they expand, while in the Ruddick-Turner experiment the temperature and salinity contrasts between the intrusions weaken as they penetrate into the opposite water mass and heat and salt are exchanged between the layers. The warm intrusions become colder as they cross the front and the cold intrusions become warmer. The intrusions are identified by their almost coinciding temperature and salinity maxima and minima. By connecting these maxima and minima in a TS diagram the diffusive and salt finger interfaces and the intermediate homogenous layers can be traced across the front and the range of the maxima and minima is limited by the initial temperature and salinity differences between the two water masses.

3   Intrusions in the Arctic Ocean

Many explanations have been forwarded for the formation of the intrusions and interleaving structures observed in the Arctic Ocean and especially in the Atlantic layer. These intrusions were discussed by *Perkin and Lewis* (1984) based on the EUBEX (EUrasian Basin Experiment) observations in 1982, and they suggested that the intrusions arose from interactions between Atlantic water newly entered through Fram Strait and Arctic Atlantic water that had spent a considerable time within the Arctic Ocean. A different explanation was offered by *Quadfasel et al*. (1993), who proposed that the intrusions were created by dense shelf outflows, especially from the Laptev Sea, and then advected along the Nansen Basin towards Fram Strait. A similar view was adopted by *Rudels et al*. (1994), however, because of the presence of intrusions over a large depth range and their regular appearance Rudels et al. assumed that the two Atlantic water inflow branches, the Fram Strait branch and the Barents Sea branch, meet at the Kara Sea continental slope and start to interact, creating intrusions with alternating diffusive and salt finger interfaces. The intrusions are then advected with the boundary current as they expand, but as the boundary current reaches the Laptev Sea a part, comprising both branches, separates from the slope and returns towards Fram Strait in the Nansen Basin and along the Gakkel Ridge (Fig. 2). The intrusions have by then released most of the

potential energy stored in their unstable property distributions and have become fossil and are passively advected with the mean circulation. This interpretation considers the intrusions and the interleaving as striking features in the Arctic Ocean water column but does not give them any major role in advecting water masses in the Arctic Ocean. By contrast, *Carmack et al.* (1997, 1998) regarded the formation and expansion of intrusions as an important process in actively spreading the heat from the boundary current at the slope into the interior of the different Arctic Ocean basins. These different views are difficult to reconcile, and in a study of the intrusions in the Eurasian Basin (*Rudels et al.*, 1999) the authors could not agree on where the intrusions were formed and how they developed, and two different interpretations of the formation and of the importance of the interleaving in the Arctic Ocean had to be formulated.
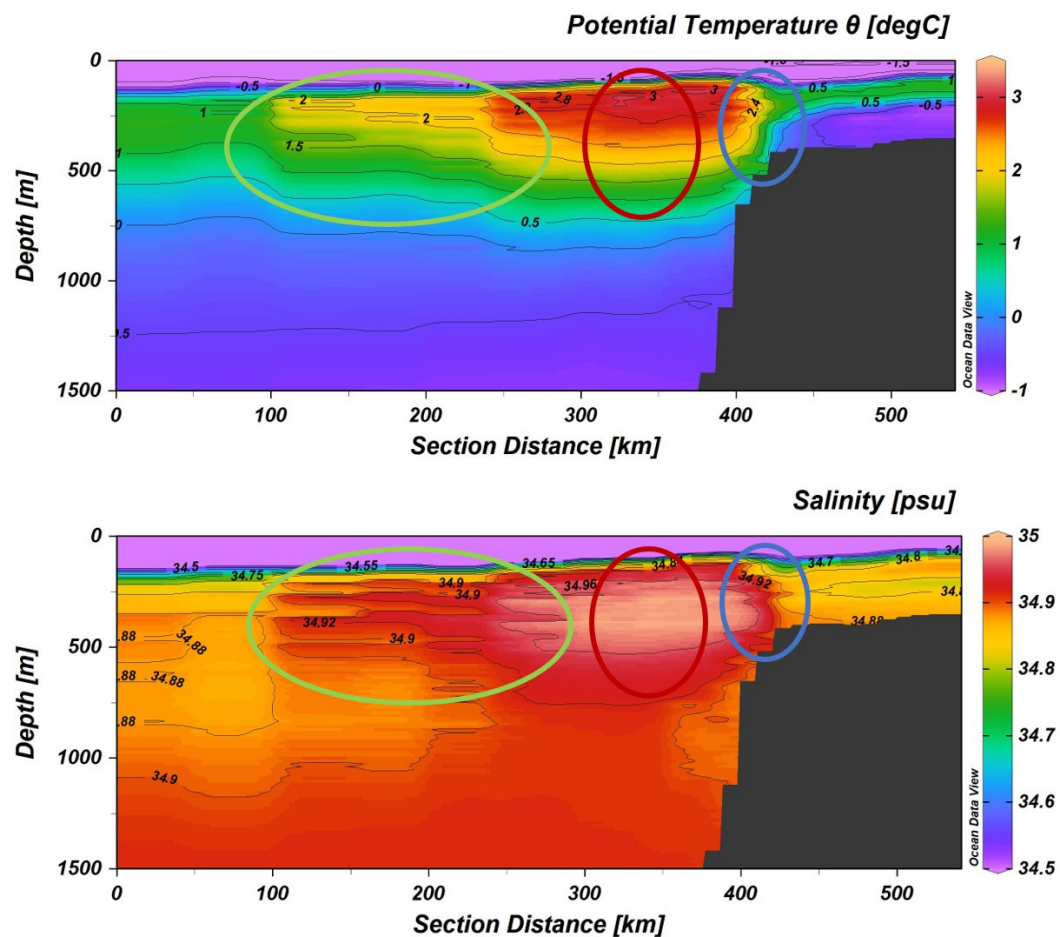

Fig. 2a. Potential temperature and salinity sections taken from the eastern Kara Sea shelf across the Nansen Basin in 2007. Interleaving and intrusions are observed on both sides of the warm, saline core of the Fram Strait inflow branch (red ellipses), at the continental slope between the Barents Sea branch (blue ellipses) and the Fram Strait branch and in the interior of the Nansen Basin. Note the wavy shape of the intrusions in the interior (green ellipses).
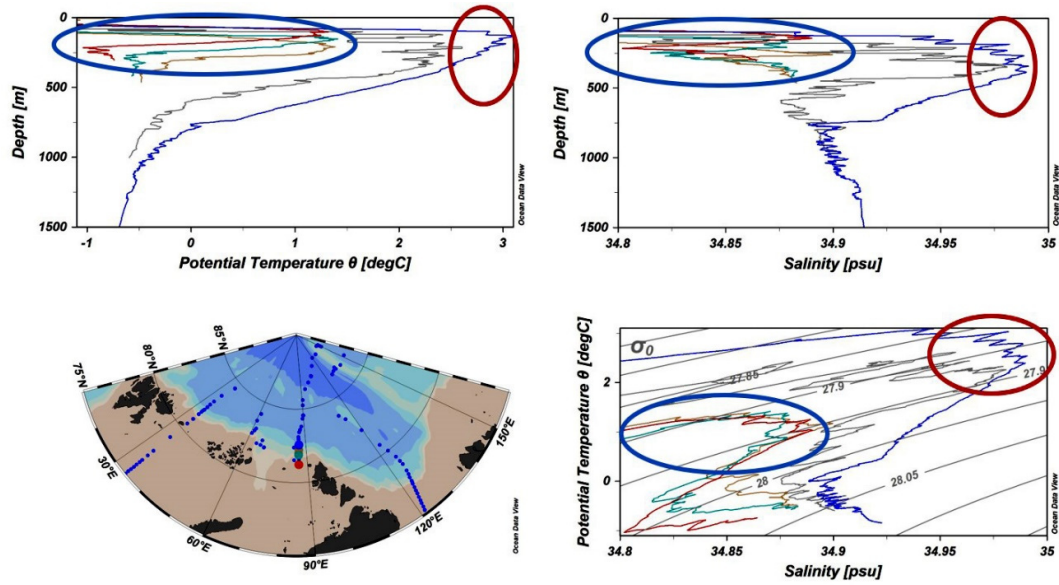
Fig. 2b. Potential temperature and salinity profiles and TS curves from the same section at the continental slope. The warm Fram Strait core is indicated by red ellipses, the Barents Sea branch by blue ellipses. Intrusions are seen between the two branches. The section and the station positions are indicated on the map.
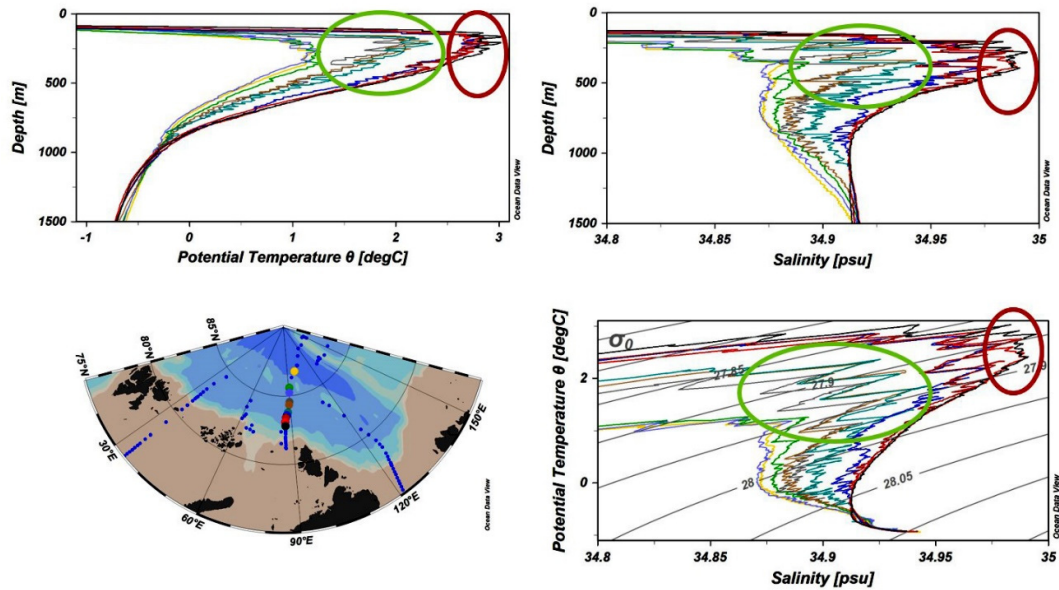

Fig. 2c. Potential temperature and salinity profiles and TS curves from the same section but in the interior of the basin. The warm Fram Strait core is indicated by red ellipses and the intrusions are indicated by green ellipses. The amplitudes of the intrusions are larger at the slope, Fig. 2b, than in the interior of the basin, and the vertical temperature and salinity gradients at the salt finger interfaces are less sharp than at the diffusive interfaces in the interior of the basin. The section and the station positions are indicated on the map.

Most studies have concentrated on intrusions present in the Atlantic layer above the temperature maximum, where the temperature distribution is unstable and infinitesimal disturbances can grow, creating intrusions (*Carmack et al.*, 1997, 1998; *Walsh and*

Carmack, 2002, 2003). *Walsh and Carmack* (2003) considered the lateral heat gradient, formed by the warm boundary current moving along the continental slope, as akin to the heating experiments by *Thorpe et al.* (1969) and proposed that the heat in the boundary current creates layers that expand into the interior of the basins, extending over distance of 2000 km and providing a strong lateral input of heat to the interior of the basin. *Bebieva and Timmermans* (2016) examined vertical and lateral temperature and salinity gradients in the diffusively unstably stratified water column above the temperature maximum and suggested that increases in the gradients by internal wave or eddy motions could lead to either formation of staircases, where the vertical fluxes dominate, or intrusions, favoring lateral exchanges.

Many, perhaps most, of the interleaving structures are, however, found in depth ranges where both components are stably stratified, mainly between the temperature maximum and the salinity maximum of the Atlantic layer, but also in the deeper layers of the Eurasian Basin below the salinity minimum. Weaker intrusions have also been observed in the Eurasian Basin between the salinity maximum and the salinity minimum, where salinity is unstably stratified. This has led to suggestions that other processes, which could generate intrusions in water columns stably stratified in both properties, might be active. *Merryfield* (2002) examined if differential diffusion, the fact that heat diffuses faster than salt, could create intrusions also when both heat and salt are stably stratified, and proposed that the deep intrusions present below the salinity minimum in the Eurasian Basin were created by this mechanism. However, he found that their growth rates were comparatively slow, 1 to 2 years. *Kuzmina et al*. (2011) examined the ideas proposed by *Walsh and Carmack* (2003) and *Merryfield* (2002), and also considered the possibility that the baroclinicity of the velocity field at the front (*May and Kelley*, 1997, 2002) could, in combination with differential diffusion, lead to a more rapid formation of the intrusions in the stable-stable situation. *Kuzmina et al*. (2011) also estimated exchange coefficients for the lateral transports in the intrusions.

There are some conceptual problems with descriptions of interleaving created by small disturbances at a front with laterally density compensating gradients of temperature and salinity. The most important objection is that this initial configuration is but rarely, or perhaps never, observed. In the Arctic Ocean more or less distinct interleaving structures are found almost everywhere, but the presumed initial state is not found. In the case of the strongest front present in the Arctic Ocean, that created at the confluence of the warm Fram Strait branch and the colder Barents Sea branch at the Kara Sea slope, the two branches come in direct contact with each other and intrusions are formed almost immediately (Fig. 2). Furthermore, the intrusions are expected to increase the mixing between the warm boundary current and the interior of the basins, but to create the initial density compensating lateral temperature and salinity gradients would require a mechanical mixing so strong that the contribution from the double-diffusively driven intrusions to the redistribution of heat from the boundary to the interior of the basin would be decidedly minor. The release of potential energy could decrease the entropy of the front by creating the interleaving layers, but the transport of heat and salt across the front by the

intrusions would be but a fraction of that already accomplished by the mechanical mixing in creating the lateral, density compensating gradients.

4   *A conceptual approach to estimate the intrusion thickness at a narrow front*

In the *Ruddick and Turner* (1979) model the layer thickness is estimated based on the final stratification after the layers have formed, and it is difficult to understand how the waters, when they start to interleave, can select the appropriate layer thickness. It would be more satisfactory, if the layer thickness could be estimated from the initial gradients rather than from the final configuration. We therefore explore the *Ruddick and Turner* (1979) approach in a very idealized, many would say unrealistic, initial situation. Two water masses are brought into contact, initially a conducting vertical wall may be imagined present between the two waters, but in the ocean the function of the wall is taken over by the slower diffusion of salt. The water masses are linearly stratified in both temperature and salinity and there are no density gradients across the front. As an illustration the stable-stable configuration is first examined (Fig. 3).

Double-diffusive convection is, regardless of the initial temperature and salinity distributions, diffusive, salt finger or stable-stable, initiated by the diffusion of heat and in contrast to *Ruddick and Turner* (1979) we here try to determine the vertical scale of the intrusions from the initial temperature difference across the front and the vertical density gradient. In the idealized situation drawn in Figure 3 heat is diffused (conducted) across the front and the water on the cold side becomes warmer and that on the warm side colder. The waters in boundary layers adjacent to the front then sink on the warm side and rise on the cold side. However, the motion in the boundary layers can only continue as long as there is a temperature difference across the front. When the temperature of the waters adjacent to the front has become equal the motion stops (Fig. 3). The water on the cold side is then less dense than that on the warm side, and if the waters cross the front, the water from the cold side would move above the water from the warm side. The maximum thickness of the interleaving layers is controlled by the density difference between the parcels at the front, $2\Delta\rho$, and it is assumed that the density changes in the boundary layers are antisymmetric, the density of the less dense parcel is $\rho - \Delta\rho$ and the density of the denser parcel $\rho + \Delta\rho$ (Fig. 3).
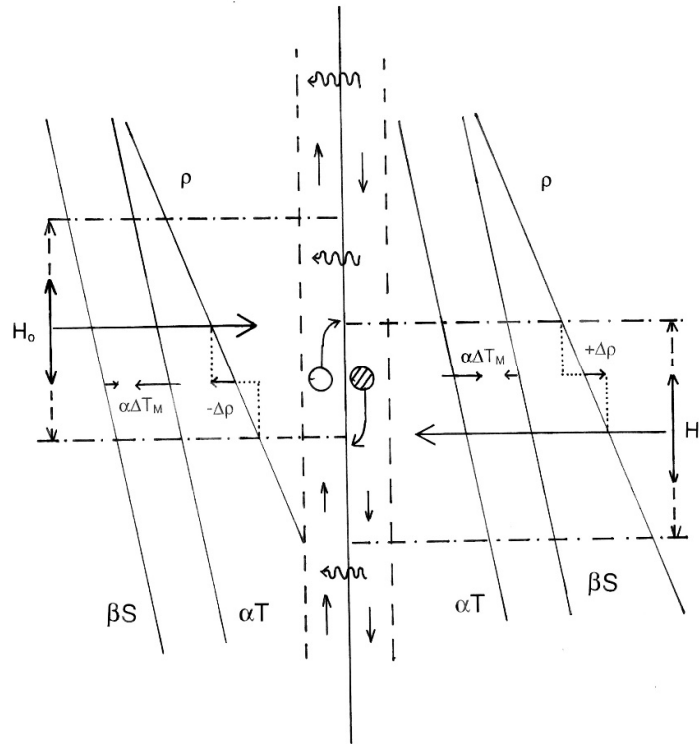
Fig. 3. Schematics showing the initial, linear density profiles due to temperature (αT) and salinity (βS) and total density (ρ) on both sides of an infinitesimally thin front. The water masses A and B are stable in both properties and no horizontal density gradients are present. The wavy arrows show the heat diffusion across the front and the broken lines indicate the created boundary layers. The colder water to the left becomes warmer and rises, the warmer water to the right sinks. Two parcels, one on each side of the front that have attained the same temperature, are indicated as circles, the parcel with increased density is shown darker. The small horizontal arrows at the profiles indicate the differences in αT, βS and ρ between the displaced parcels and their surroundings. If the parcels penetrate through the front into the opposing water mass, they will enter at the corresponding density levels, which, because of the symmetry of the density changes, coincide with the initial density level of the opposing parcels. The water entering after the penetrating parcel has the same mean density but the intrusion thickness H_o is half of the depth interval from which the water is drawn due to the "lock-exchange" flow generated as the waters interleave.

There is only little water present in the boundary layers, but the flow across the front selects the vertical scale of the interleaving and opens passages for intrusions that bring water from the two sides across the front. The thickness of the intrusions, here defined as the part moving in one direction, is given by $2\Delta\rho(grad\rho)^{-1}$ where $grad\rho$ is the vertical density gradient in the water columns, but the waters crossing the front are drawn from a layer $4\Delta\rho(grad\rho)^{-1}$, twice as thick as the intrusions, which expands into the opposing water mass in an energy conserving lock-exchange flow (*Benjamin*, 1968). Considering only water columns, where the vertical temperature and salinity gradients are equal on both sides of the front, the TS curves of the two water columns are parallel in an αT-βS diagram with αT increasing downwards and scaled as $\alpha T = \beta S$ (Fig. 4). The initial

temperature and salinity differences between the water column along an isopycnal are given by $\alpha\Delta T_o = \beta\Delta S_o$ and the density change in the boundary layer due to the heating becomes $\alpha\Delta T_M$;
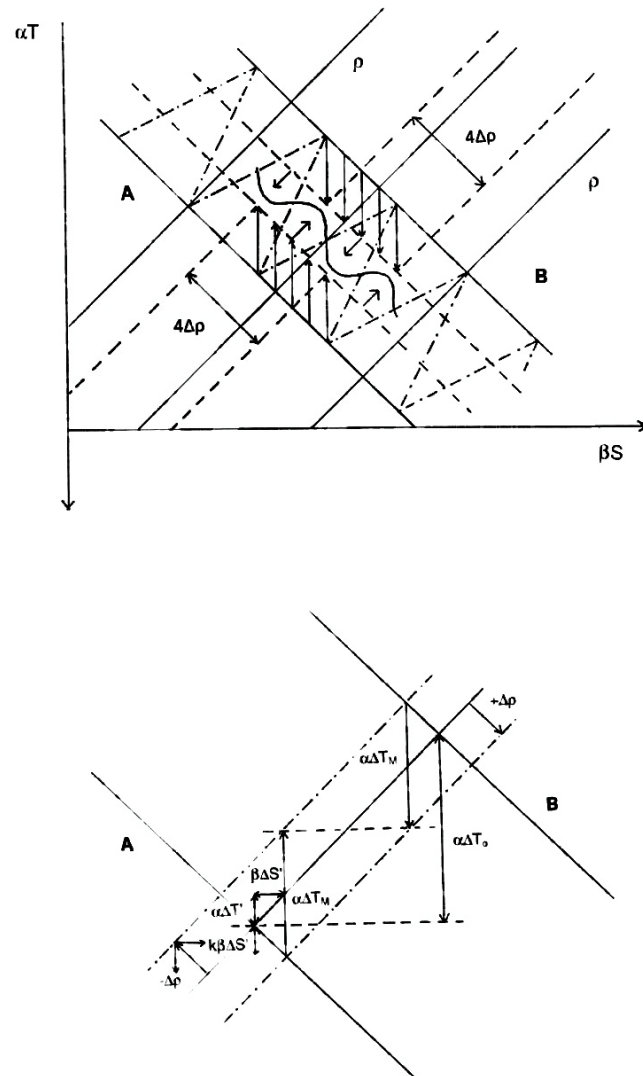

Fig. 4. The upper panel shows the same situation as in Fig. 3 but in a αT-βS diagram. The vertical arrows show the temperature evolution in the boundary layer, due to heat diffusion, from the initial water mass characteristics (solid lines) to the maximum temperature change (broken lines). The vertical upward and downward pointing arrows are anti-symmetric around the ambient density. The broken lines parallel to the isopycnals indicate the density ranges from which the interleaving layers are drawn. The arrows, showing the interleaving of the water masses, are located at the mean density of the layers. The dash-dot line shows the T-S curve of the layering after the layers have been homogenised. The lower panel shows a blow up of the temperature difference across the front, $\alpha\Delta T_o$, the mean temperature change of a parcel at the front, $\alpha\Delta T_M$. k is the slope of the water masses in the αT-βS diagram. $\Delta\rho = \alpha\Delta T_M/2$ is half the initial density range of the interleaving layers and half the density difference between two neighbouring layers. The figure defines the $\alpha\Delta T'$ and $\beta\Delta S'$ used in the text. Note that $\alpha\Delta T' = k\beta\Delta S'$.

$$2\rho_*^{-1}\Delta\rho = \alpha\Delta T_M = \frac{\alpha\Delta T_o}{2} + \alpha\Delta T' = \frac{\alpha\Delta T_o}{2} + k\beta\Delta S' \tag{2}$$

$\alpha\Delta T'$ and $\beta\Delta S'$ are related to the slope $k = \tan(\alpha\Delta T/\beta\Delta S)$ of the water columns in the αT-βS diagram (Fig. 4). However, $2\rho_*^{-1}\Delta\rho$ is also equal to;

$$2\rho_*^{-1}\Delta\rho = \beta\Delta S_o - 2\beta\Delta S' \tag{3}$$

Eliminating $2\rho_*^{-1}\Delta\rho$ and introducing the slope k gives;

$$\beta\Delta S' = \frac{\alpha\Delta T_o}{2(2+k)} \tag{4}$$

The change in temperature, $\alpha\Delta T_M$, can then be written as;

$$\alpha\Delta T_M = \frac{\alpha\Delta T_0}{2} + \frac{k\alpha\Delta T_o}{2(2+k)} = \frac{\alpha\Delta T_o}{2}\left(1 + \frac{k}{(2+k)}\right) = \alpha\Delta T_o\left(\frac{1+k}{2+k}\right) \tag{5}$$

This implies that $\alpha\Delta T_M = \alpha\Delta T_o$, if the water columns are stratified only in temperature ($k = \infty$) and $\alpha\Delta T_M = \frac{1}{2}\alpha\Delta T_o$ if they are stratified only in salinity ($k = 0$). When the density contributions from temperature and salinity are equal ($k = 1$) $\alpha\Delta T_M = 2/3\ \alpha\Delta T_o$. If the temperature stratification is unstable but the vertical gradients on each side of the front are equal, the temperature change is still given by Equation (5), but now k ranges between 0 and -1, and $\alpha\Delta T_M$ becomes smaller as the TS slope approaches that of the isopycnals (Fig. 5). When the water columns are neutrally or unstably stratified in salinity, no temperature inversions and no diffusive interfaces are formed (Fig. 5). This was pointed out by *McDougall* (1986) in a critique of the Ruddick-Turner experiment, claiming that the Ruddick-Turner configuration could not generate diffusive interfaces in the ocean. Furthermore, it is not possible to fulfill both the symmetry condition for the density changes and attain the same temperature across the front when $-2 < k < -1$.

To determine the temperature and salinity steps between the layers as they start to interleave the property steps across the front have to be corrected for the differences in mean temperature and salinity between the layers above and below the interfaces. The changes in density in the vertical boundary layers are $\pm\rho_*^{-1}\Delta\rho = \pm\frac{1}{2}\alpha\Delta T_M$ and separating the density change into the corresponding temperature and salinity changes using $\alpha\Delta T_0 = \beta\Delta S_o$ leads to;

$$\frac{\alpha\Delta T}{2} = \frac{\alpha\Delta T_M}{2}\left(\frac{k}{1+k}\right) = \frac{\alpha\Delta T_o}{2}\left(\frac{1+k}{2+k}\right)\left(\frac{k}{1+k}\right) = \frac{\alpha\Delta T_o}{2}\left(\frac{k}{2+k}\right) \tag{6}$$

$$\frac{\beta\Delta S}{2} = \frac{\alpha\Delta T_M}{2}\left(\frac{1}{1+k}\right) = \frac{\alpha\Delta T_o}{2}\left(\frac{1+k}{2+k}\right)\left(\frac{1}{1+k}\right) = \frac{\beta\Delta S_o}{2}\left(\frac{1}{2+k}\right) \tag{7}$$

As the layers start to interleave the salinity and temperature steps at the diffusive interfaces then become:

$$\alpha\Delta T_D = \alpha\Delta T_o\left(1 - \frac{k}{2+k}\right), \qquad \beta\Delta S_D = \beta\Delta S_o\left(1 + \frac{1}{2+k}\right) \tag{8}$$

And the corresponding steps at the salt finger interfaces are;

$$\alpha\Delta T_F = \alpha\Delta T_o\left(1 + \frac{k}{2+k}\right), \qquad \beta\Delta S_F = \beta\Delta S_o\left(1 - \frac{1}{2+k}\right) \tag{9}$$
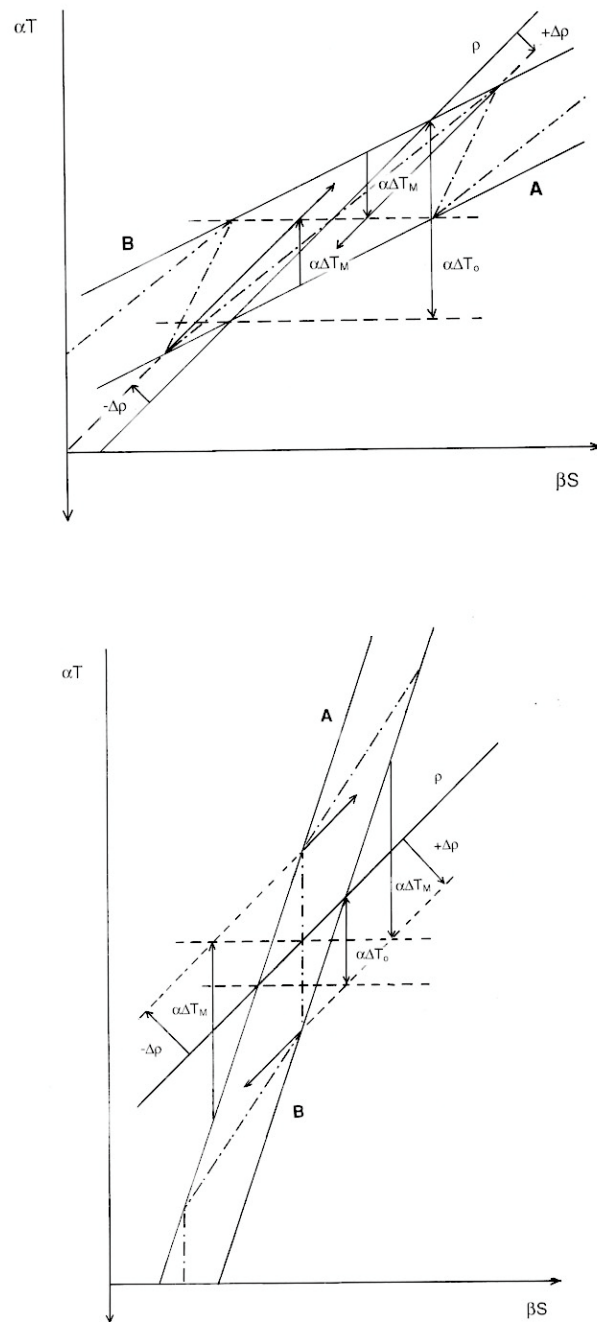
Fig. 5. The upper panel shows the evolution of intrusions in an αT-βS diagram for the case when the background stratification is unstable in the diffusive sense, while the lower panel shows the evolution when the background stratification is unstable in the salt finger sense. The difference in property steps at the diffusive and salt finger interfaces is large, the steps at the diffusive interface being larger, when the background stratification is unstable in the diffusive sense. The salt finger interface might then overturn. When the background stratification is unstable in salinity, no inversions in temperature are created, if the motions in the boundary layer continue until the maximum temperature change is reached. The change in temperature, $\alpha \Delta T_M$, is also much larger than the initial temperature jump $\alpha \Delta T_o$. The symbols are the same as in Fig. 4.

The behavior of the steps for different stratifications can be visualized by plotting them against arctan(k) (Fig. 6). The temperature steps on the two interfaces are equal to $\alpha\Delta T_o$ for k = 0 and when the stratification is stable in both properties (k ≥ 0). $\alpha\Delta T_D$ decreases to zero when k → ∞ while $\alpha\Delta T_F$ increases to $2\alpha\Delta T_o$. The salinity steps are $\beta\Delta S_D = 3/2\beta\Delta S_o$ and $\beta\Delta S_F = 1/2\beta\Delta S_o$ for k = 0, and they both approach $\beta\Delta S_o$ as k goes to infinity. When the background stratification is unstable in the diffusive sense (−1 < k <0, or −45° < arctan(k) <0°), both $\alpha\Delta T_D$ and $\beta\Delta S_D$ increase towards $2\alpha\Delta T_o = 2\beta\Delta S_o$, and $\alpha\Delta T_F$ and $\beta\Delta S_F$ both go to zero when k approaches −1. For k < −1 the background stratification is unstable in the salt finger sense, but both criteria, the same temperature in the boundary layer and antisymmetric density change relative to a mean isopycnal, can only be fulfilled for k < −2. $\alpha\Delta T_D < 0$ and no temperature inversions and no diffusive interfaces are formed. $\beta\Delta S_F$ also goes below zero before k reaches −2 and then no salinity inversions are created. As k approaches −2 both $\alpha\Delta T_F$ and $\beta\Delta S_D$ go to positive infinity, while $\alpha\Delta T_D$ and $\beta\Delta S_F$ approach negative infinity, and when k→−∞ $\alpha\Delta T_F$ and $\beta\Delta S_F$ become 2 and 1 respectively.

The stability ratios $R\rho^D$ and $R\rho^F$ at the diffusive and salt finger interfaces reflect these changes. $R\rho^F$ remains constant for the entire range of k, while $R\rho^D$ decreases from positive infinity at k = ∞ to 3/2 at k = 0 and 1 at k = −1. If k goes to −∞ $R\rho^D$ continues towards negative infinity, indicating absence of diffusive interfaces. For k close to −1, $R\rho^F$ goes to positive infinity implying the disappearance of the salinity inversions (Fig. 6). It is then obvious that this approach does not well describe the formation of intrusions, when the background stratification is in the salt finger sense, but this situation is not common in the Arctic Ocean. By contrast the basic features of the intrusions created where the stratification is unstable in the diffusive sense or where both components are stably stratified appear better described.

Because of the density change $2\Delta\rho$ the maximum distance the parcels in the boundary layer move in the stratification becomes $2\Delta\rho(\mathrm{grad}\rho)^{-1}$ and as the density change is equal to $\alpha\Delta T_M$ the thickness of the layers becomes;

$$H_o = \frac{\alpha\Delta T_O}{\rho_*^{-1}grad\rho}\frac{1+k}{2+k} \quad with \quad \rho_*^{-1}grad\rho = \rho_*^{-1}\frac{\partial\rho}{\partial z} = \left(\frac{\partial\alpha\Delta T}{\partial z} + \frac{\partial\beta\Delta S}{\partial z}\right) \tag{10}$$

This is the maximum thickness. Assuming that the vertical density gradient is the same for different vertical salinity and temperature gradients the layer depth is controlled by the initial temperature difference across the front and the contributions of salinity and temperature to the stability. The layer thickness depends weakly on the stratification when both components are stably stratified, and approaches zero, when the temperature stratification is unstable and the stability disappears for k = −1. By contrast, unstable salinity stratification and weak stability lead to infinite layer thickness (Fig. 6d).
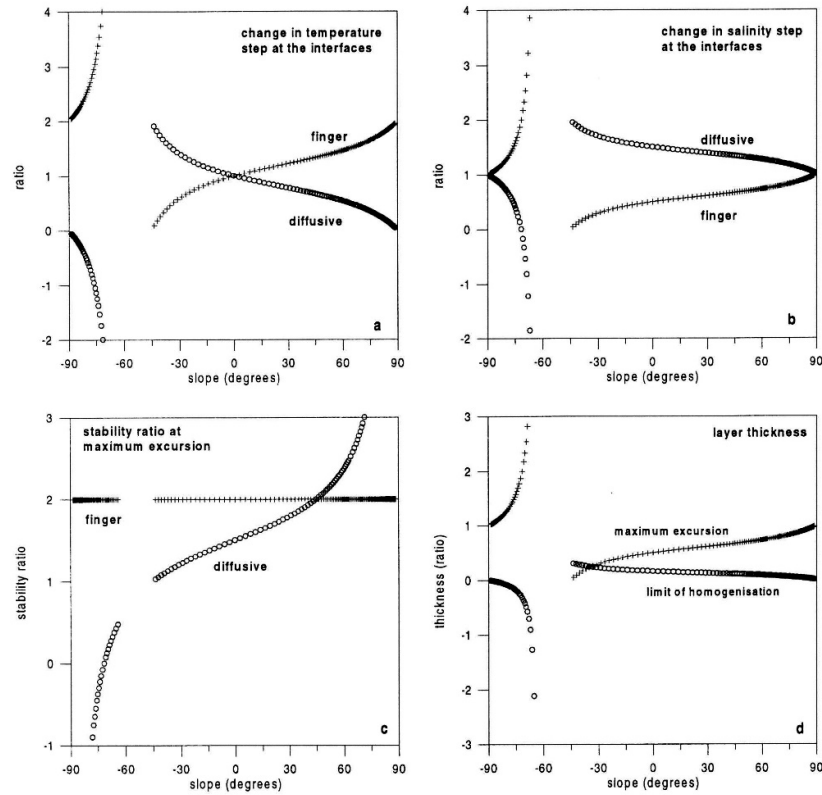
Fig. 6. (**a**) The ratio of the $\alpha\Delta T_D/\alpha\Delta T_o$ (circles) and $\alpha\Delta T_F/\alpha\Delta T_o$ (crosses) at the diffusive and salt finger interfaces for the maximum temperature change shown as functions of the slope (Arctan(k)) of the water masses in an αT-βS diagram. (**b**) The ratio of the $\beta\Delta S_D/\beta\Delta S_o$ (circles) and $\beta\Delta S_F/\beta\Delta S_o$ (crosses) at the diffusive and salt finger interfaces for the maximum temperature change shown as functions of the slope (Arctan(k)) of the water masses in an αT-βS diagram. (**c**) The stability ratio at the diffusive interface (circles) and at the salt finger interface (crosses) shown as function of the slope (Arctan(k)) of the water masses in an αT-βS diagram. (**d**) The thickness ratios $H_o/(\alpha\Delta T_o/grad\rho)$ (crosses) and $d/(\alpha\Delta T_o/grad\rho)$ (circles) plotted against the slope (Arctan(k)) of the water masses in an αT-βS diagram. H_o corresponds to the case of maximum temperature change. No convection and no homogenisation of the layers occur with a background salt finger stratification.

The interleaving layers are assumed to be homogenized by the stirring caused by buoyant parcels and/or plumes that rise and sink from the interfaces. The density anomalies in the buoyant parcels rising and sinking from the diffusive interface are given by $\delta\rho = \pi^{-1}\alpha\Delta T_D$ (*Crank*, 1956) and the distance d, which the parcel can rise becomes;

$$d = \frac{\alpha\Delta T_D}{2\pi\rho_*^{-1}grad\rho} = \frac{\alpha\Delta T_o}{2\pi\rho_*^{-1}grad\rho}\left(1 - \left(\frac{k}{2+k}\right)\right) \tag{11}$$

Here the initial gradient has been doubled to take into account the reduction in thickness as the waters penetrate across the front. It is clear that d is considerably smaller than H_o except when the temperature stratification is unstable (Fig. 6d). If the background salinity stratification is unstable, no active diffusive interfaces are formed and this approach is not valid for a background salt finger stratification.

The vertical motions induced by heat conduction at the front do not have to reach their maximum amplitude before the interleaving starts. In fact, it is highly unlikely that they do. Another possible way to estimate the density difference between the created layers is to relate their thickness, h, directly to the distance the parcels can rise and sink in the stratification, d. The temperature step at the diffusive interface, using Equation (11), then becomes;

$$\alpha \Delta T_D = h\pi(1 + k)grad(\beta S) \tag{12}$$

Since also;

$$\alpha \Delta T_D = \alpha \Delta T_o - hk\, grad(\beta S) \tag{13}$$

eliminating h gives the temperature step at the diffusive interface as;

$$\alpha \Delta T_D = \frac{\alpha \Delta T_o}{\left(1 + \frac{k}{\pi(1+k)}\right)} \tag{14}$$

The corresponding salinity step becomes from Equation (13);

$$\beta \Delta S_D = \beta \Delta S_o + \alpha \Delta T_D \frac{1}{\pi(1+k)} \tag{15}$$

Since $\alpha \Delta T_o = \beta \Delta S_o$ the stability ratios for the diffusive and salt finger interfaces are;

$$R\rho^D = \frac{\beta \Delta S_D}{\alpha \Delta T_D} = 1 + \frac{1}{\pi}, \qquad R\rho^F = \frac{\alpha \Delta T_F}{\beta \Delta S_F} = \frac{1 + \frac{2k}{\pi(1+k)}}{1 + \frac{k-1}{\pi(1+k)}} \tag{16}$$

The stability ratio for the diffusive interface is constant, ~1.3, for the entire range of k, and $R\rho^F$ is also close to 1.3 for most k, except for $-1 < k < -1/2$, where $R\rho^F$ first goes below 1 and then to negative values. This implies that when the stability is weak and the stratification is unstable in the diffusive sense, the parcels or plumes could rise indefinitely and no salinity inversions, no salt finger interfaces and no layers would form. This approach, however, does not work when the background salinity stratification is unstable, since no diffusive interfaces then are formed.

No infinitely thin fronts, and consequently no situation where horizontal heat conduction might create boundary layers such as those discusses above, exist in the ocean. The present approach has been used as a scaffolding to estimate the thickness and the properties of intrusions created at a narrow front between two different water masses with the same vertical density gradient but with different vertical gradients in temperature and salinity. The volume of water present in the introduced boundary layers is small, but in this approach the changes estimated at the boundary set the vertical scales for the layers that transport the waters from the two sides across the front. Once the scales have been found, the scaffolding can be removed.

It is, however, obvious that the derived vertical scales in most situations are too large, and the motions in the vertical boundary layers might go unstable before the

maximum displacement is reached, or scale of the layers is set by other, external disturbances with smaller vertical wavelengths that could bring the different waters far enough across the front for inversions to form and the double-diffusive transport to start. Motions that could generate such disturbances are inertial waves, which have large vertical but small horizontal wave numbers (*Toole and Giorgi*, 1981), or internal tides generated by the interaction with the barotropic tidal wave with the bathymetry at the continental slope (*Rippeth et al.*, 2015). Another possibility is that once an intrusion, by some process, has been formed, it will move into the opposite water mass as a gravity current, generating return flows above and below. In an energy conserving lock-exchange flow these return flows will have similar thicknesses as the original intrusion and its scale is imposed on the entire interleaving structure. The vertical scale of the initial disturbance determines the property steps and the stability ratios at the interfaces. These then deviate from the idealized cases discussed above, but once the scale of the initial disturbance is known, the characteristics of the interleaving can be deduced by examining the properties of the undisturbed water columns.

5 The transports across the interfaces and the spreading of the intrusions

The changes in the stratification discussed so far are due to homogenization of the waters in the different layers and only the stirring effects of double-diffusive convection have been considered. However, double-diffusive convection transports density anomalies across the interfaces, which change the densities in the intrusions and can initiate motions across the front into the opposing water mass. The double-diffusive transports are assumed described by the 4/3 flux laws, $F_{\alpha T}^D \sim \alpha \Delta T^{4/3}$ for the diffusive interfaces and $F_{\beta S}^F \sim \beta \Delta S^{4/3}$ for the finger interfaces. These 4/3 laws are similar to those that apply to high Rayleigh number convection, where the heat transport is assumed independent of the thickness of the layers and only controlled by the property steps at the interfaces (*Turner*, 1965, *Howard*, 1967). The 4/3 flux laws have been criticized (e.g. *Kelley*, 1984, 1990; *Radko*, 2013) and that exponent is slightly less, about 1.27, but we judge these laws accurate enough to be used considering all other uncertainties introduced when describing the intrusions.

For the transports through the diffusive interfaces the flux law proposed by *Foldvik and Rudels* (1996) is adopted. For $R\rho^D$ close to 1 this expression is based on theoretical considerations, while for $R\rho^D$ around 4 existing laboratory estimates, have been used. The flux ratio is also for the interval $1 < R\rho^D < 2$ taken to be constant and equal to $(\kappa_S(\kappa_T)^{-1})^{1/2} = \tau^{1/2}$.

$$F_T = C_D \left(\frac{g\kappa_T^2}{\nu}\right)^{1/3} (\alpha \Delta T)^{4/3}, \quad C_D = 0.0948 \, (R\rho)^{-1.18}, \quad Rf^D = \tau^{1/2} \approx 0.1 \quad (17)$$

Here g is the acceleration of gravity, κ_T and κ_S the diffusion coefficients of heat and salt and ν the coefficient of viscosity and $Rf^D = F_{\beta S}^D (F_{\alpha T}^D)^{-1}$. There is no large difference between this law and the more commonly used law formulated by *Kelley* (1990), and the result would be similar if Kelley's formulation had been used.

For the salt finger fluxes the expression proposed by *Kunze* (1987, his Figure 7) will be applied with some simplifications. The transports show a weak linear increase as $R\rho^F$ decreases towards 1.5 and for $R\rho^F$ less than 1.5 both salt and heat transports start to increase more rapidly, while the buoyancy flux remains constant. Since the buoyancy flux is the dynamically important one, the increase with decreasing $R\rho^F$ is ignored and $F_{\beta S}{}^F$ and $F_{\alpha T}{}^F$ are given by;

$$F_{\beta S}^{F} = (0.08 - 0.005 R\rho^{F})(\kappa_{T}g)^{1/3}(\beta\Delta S)^{4/3}; \quad F_{\alpha T}^{F} = \gamma F_{\beta S}^{F}; \quad \gamma = 0.7 \qquad (18)$$

Another difference from *Kunze* (1987) is that the flux ratio $F_{\beta S}{}^F (F_{\alpha T}{}^F)^{-1} = Rf^F = \gamma = 0.7$ is independent of $R\rho^F$. The value is the mean between the values at $R\rho^F = 1.1$ and $R\rho^F = 1,5$ given by Kunze. Equations (17) and (18) give the transport of density anomaly, not the buoyancy flux, the difference being the acceleration of gravity g = 9.81 (Fig. 7).
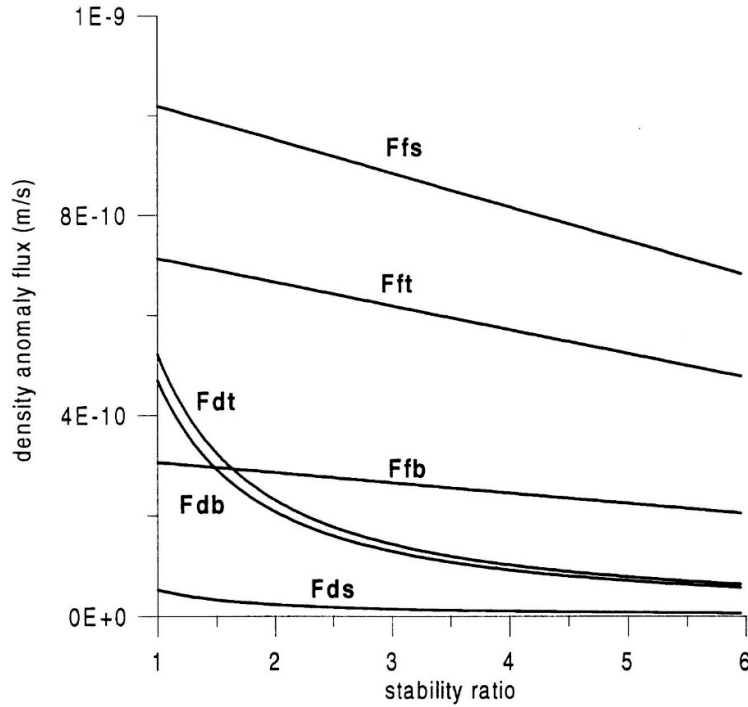

Fig. 7. The dependence of the employed density anomaly flux laws on the stability ratio. Ffs (salt finger flux of salt), Fft (salt finger flux of heat), Ffb (salt finger flux of buoyancy). Fds (diffusive flux of salt), Fdt (diffusive flux of heat), Fdb (diffusive flux of buoyancy).

The laboratory flux laws often overestimate the double-diffusive transports measured in the ocean by other techniques, but this might be due to insufficient resolution of the temperature and salinity profiles. The observed temperature and salinity steps could in reality consist of several smaller steps and the transports would then be correspondingly reduced. However, observational techniques are steadily improving, and in the ice-covered Arctic Ocean the vertical movements at the surface are small and ITPs (Ice

Tethered Platforms) profiling from the ice, as well as bottom deployed profilers might already be able to resolve the temperature and salinity profiles down to the required 0.01–0.05 m scale.

To simplify the matter the stable-stable situation where the vertical salinity and temperature gradients both contribute equally to the stability is considered. This is also the situation most frequently encountered in the interleaving structures in the Arctic Ocean. Applying the adopted flux laws the rates of change $\dot{\delta}$ of temperature and salinity in the layers are given by;

$$\dot{\delta}\alpha T = \frac{-\left(F^D_{\alpha T}+\gamma F^F_{\beta S}\right)}{h} \; ; \qquad \dot{\delta}\beta S = \frac{\left(\tau^{1/2}F^D_{\alpha T}+F^F_{\beta S}\right)}{h} \tag{19}$$

if the layer is a cold intrusion bounded by a finger interface above and a diffusive interface below. The layer thickness is h and the convention that positive $\delta\alpha T$ implies a density increase has been adopted. The changes with a diffusive interface above and a finger interface below, a warm intrusion, are antisymmetric to those given in Equation (19).

The stability ratios at the salt finger and diffusive interfaces are defined as;

$$R\rho^F = \frac{(\alpha\Delta T_P - 2|\delta\alpha T|)}{(\beta\Delta S - 2|\delta\beta S|)} \; ; \qquad R\rho^D = \frac{(\beta S_P - 2|\delta\beta S|)}{(\alpha\Delta T - 2|\delta\alpha T|)} \tag{20}$$

Here $\beta\Delta S_P$ and $\alpha\Delta T_P$ are the property steps of the passive component at the interface. The changes in the properties can be written as flux ratio, Rf for the layers;

$$\frac{\dot{\delta}\alpha T}{\dot{\delta}\beta S} = \frac{F_{\alpha T}}{F_{\beta S}} = -Rf \tag{21}$$

The minus sign is introduced to make Rf positive. The density anomaly flux then becomes;

$$F_B = \left(F_{\alpha T} - F_{\beta S}\right) = F_{\alpha T}(1 - Rf^{-1}) \tag{22}$$

The initial stability ratios $R\rho_o$ at the diffusive interface and at the salt finger interface are equal and smaller for smaller initial thickness of the layers. The time evolutions of $\alpha\Delta T$ and $\beta\Delta S$ and $\alpha\Delta T_P$ and $\beta\Delta S_P$, the subscript p indicating the stable property step, are shown in Fig. 8 for different initial stability ratios. When the heat transport dominates, the density of a warm intrusion increases and that of a cold intrusion decreases, while if the salt transport is the largest the warm intrusions become less dense and the cold intrusions denser. For small stability ratios the heat flux dominates, and for $R\rho_o < 1.04$ the stabilizing $\alpha\Delta T_P$ at the salt finger interface becomes smaller than the destabilizing $\beta\Delta S$ and the salt finger interface overturns. For larger $R\rho_o$ the stability of the salt finger interface goes through a minimum and then starts to increase. This agrees with the theoretical and laboratory study by *Ruddick* (1984). He used salt and sugar as diffusive substances and observed that for small enough $R\rho_o$ the salt finger interface overturned.
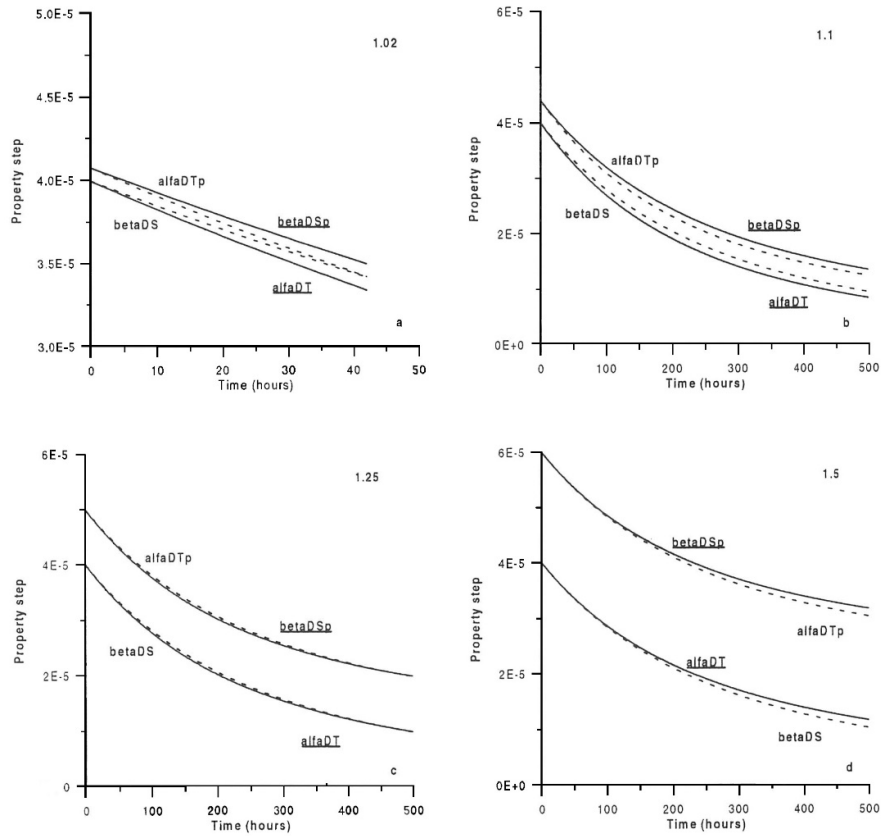
Fig. 8. The changes in active and passive property steps Δ and Δ_P (note that $\Delta_P > \Delta$). Solid lines indicate the diffusive steps $\Delta T/\Delta T_o$ and $\Delta S_P/\Delta S_o$ and broken lines the salt finger steps $\Delta S/\Delta S_o$ and $\Delta T_P/\Delta T_o$ as functions of time for different initial $R\rho$. The steps belonging to the diffusive interface are underlined. a) $R\rho$=1.02, b) $R\rho$=1.1, c) $R\rho$=1.25, d) $R\rho$=1.5. The salt finger interface overturn for $R\rho$=1.02.

The change of flux ratio for different initial stability ratios as function of $R\rho^D$ is shown in Fig. 9. The heat transport is larger than the salt transport for small $R\rho^D$, which leads to more rapid changes in the stability ratio at the diffusive interface compared to the salt finger interface. In general, no overturning of the salt finger interface takes place, and the heat and salt fluxes evolve towards $Rf = 0.8$ to 0.9. The intrusions thus change from being dominated by the heat transport through the diffusive interfaces to a stage when the salt finger fluxes become the largest. The $R\rho^D$ for which the crossover takes place depends upon the initial stability ratio. The smaller the initial value the smaller is the $R\rho^D$ for which the transition occurs. Layers with initial small $R\rho$ then eventually appear to be more dominated by salt finger fluxes than those with larger initial stability ratios. An $Rf \sim 0.8$-0.9 is actually close to the flux ratios often deduced from observations of intrusions and interleaving in the ocean.
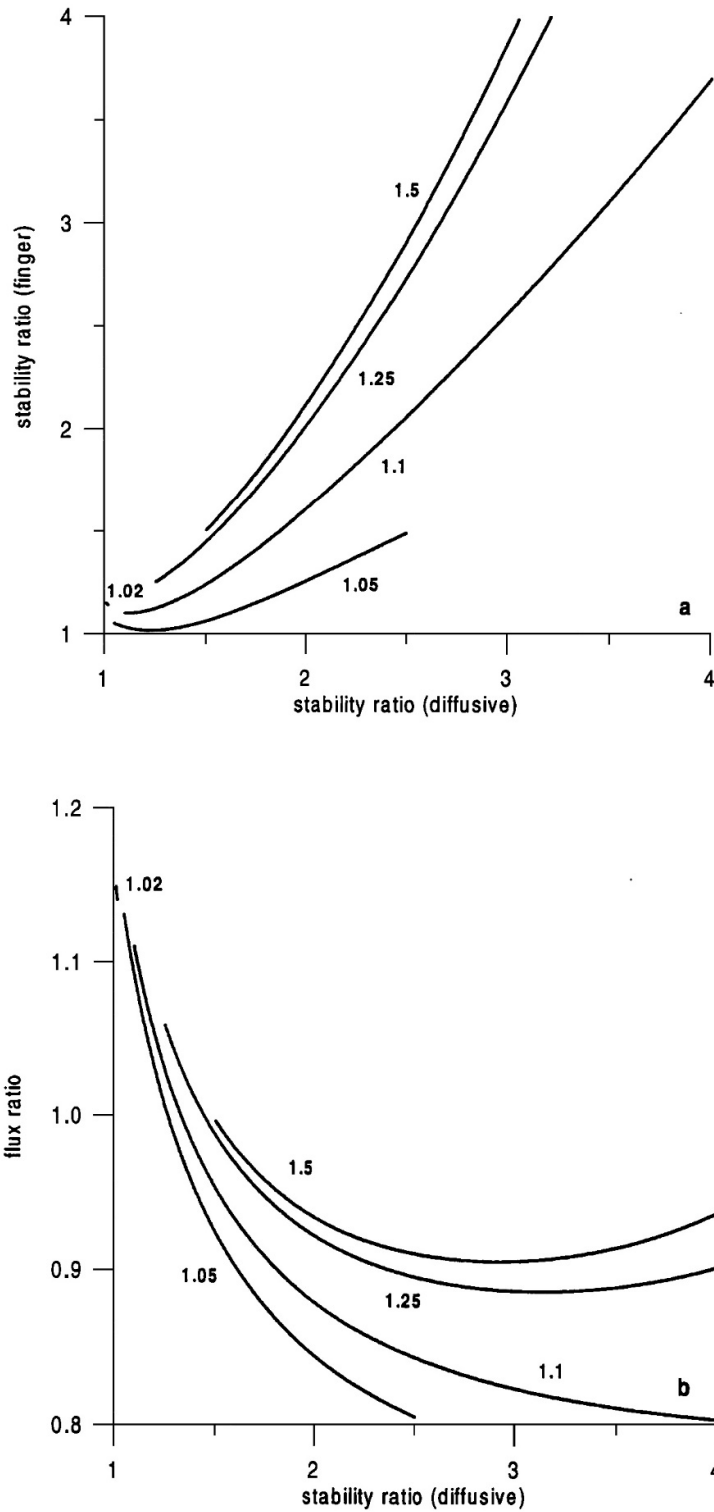
Fig. 9. **a)** The evolution of the stability ratios with time for different initial $R\rho^F = R\rho^D$. **b)** The flux ratio Rf $= F_{\alpha T}(F_{\beta S})^{-1}$ in the layers as function of $R\rho^D$, the stability ratio at the diffusive interface.

6   *Characteristics of intrusions and layers in the Arctic Ocean*

To find, how these estimates relate to interleaving structures in the Arctic Ocean, we examine layers observed in the Nansen Basin in 1991, 1995 and 1996. The property steps and the stability ratios of the layers are expected to evolve, the step becoming smaller and the stability ratios larger. By contrast the background density gradient and the layer thickness should remain fairly constant. This implies that if $(h/\alpha\Delta T)$ and $(h/\beta\Delta S)$ for the diffusive and salt finger interfaces respectively are plotted against $R\rho$, their values should increase with increasing $R\rho$. Moreover, if it is assumed that the initial low stability ratio obtained in Equation (16) is somehow representative, the observed relations could be extrapolated to this low $R\rho$ value. With the density gradient known, the initial $\alpha\Delta T_D$ and $\alpha\Delta T_o$, $\beta\Delta S_D$ and $\beta\Delta S_o$ could then be estimated from Equations (12) and (14).

To find the temperature and salinity steps and the layer thickness from the observations, the depths and the salinity and temperature of the maxima and minima were estimated, and the differences computed at each station. The observed steps are often asymmetric, and the distance between maximum and minimum (the salt finger steps) are frequently much larger than the distance between minima and maxima (the diffusive step) (see Fig. 2 above). If we assume that the layers are formed by disturbances generated at a front, these steps should initially be equal. This implies that the interfaces were originally located at the centre of the unstable salinity and the unstable temperature gradient respectively. The observed differences in thickness are then caused by a gradual thickening of the interfaces. The diffusive interface is kept thin by the convection of buoyant parcels from the interface. The salt finger interface, however, would spread more rapidly due to the transfer of mass through the interface between the layers (Fig. 2). To take this into account, at least provisionally, we define the thickness, h, of a layer as 1/2 the distance between the maximum and the minimum plus 1/4 of the distances between the maximum and the minimum above, and between the minimum and the maximum below. This may not be the most sophisticated way to proceed, and since the distance between maximum and minimum is larger, it may still bias towards larger $(h/\beta\Delta S)$ than $(h/\alpha\Delta T)$ (Fig. 10).
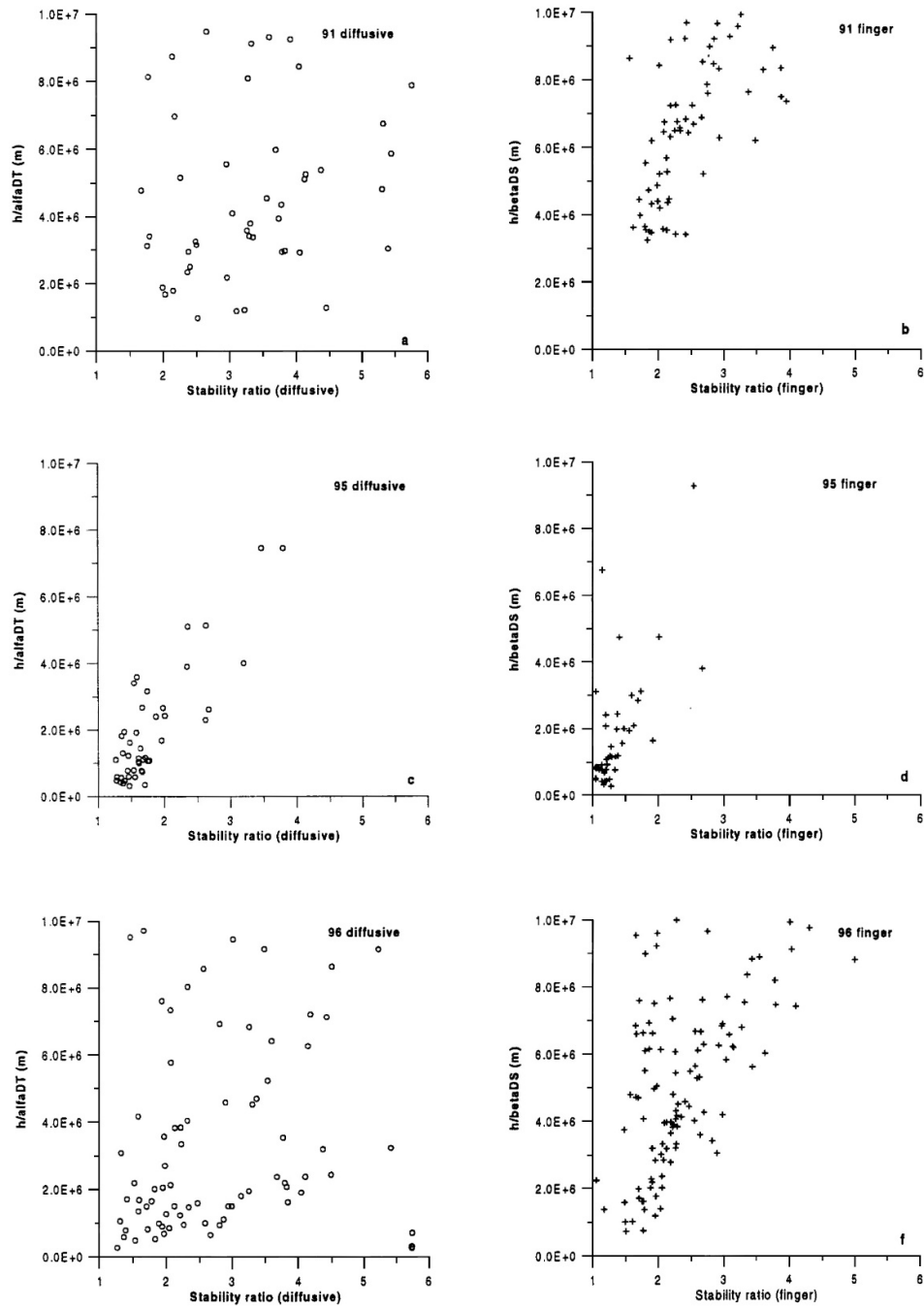
Fig. 10. The ratio (h/α∆T) plotted against $R\rho^D$ at the diffusive interface (left panel) and the ratio (h/β∆S) plotted against $R\rho^F$ at the salt finger interfaces (right panel) for the interleaving structures observed in the Arctic Ocean in 1991 (top), 1995 (centre) and 1996 (bottom). h is the thickness of the layer (see text) and ∆T and ∆S are the observed steps between the maxima and minima.

The salt finger interfaces do not attain as large Rρ as the diffusive interface, in agreement with initially stronger diffusive fluxes. For the 1995 observations, which are from the frontal zone north of Severnaya Zemlya, the $R\rho^F$ are in some instances very close

to 1 and to instability (the data have been cut at the axis and no $R\rho^F < 1$ are shown). The values of $(h/\alpha\Delta T)$ and $(h/\beta\Delta S)$ increase with increasing $R\rho$, and since the thickness of the layers is not likely to change with time, this indicates that the steps were initially larger. The scatter of the data points is enormous and too much should not be concluded from these diagrams. However, Figure 10 does suggest initial $R\rho^D$ of 1.2 for the diffusive interface and that $(h/\alpha\Delta T)$ initially is about $0.3\text{-}0.5\times10^6$ m. The density gradient within the Arctic Ocean is around 0.4×10^{-3} kgm^{-4}, but this value could easily range from 1×10^{-3} kgm^{-4} at shallower levels and 0.15×10^{-3} kgm^{-4} in the deep. With $\rho_* = 1000$, $\rho_*\alpha\Delta T/h$ becomes $\sim2.5\times10^{-3}$ kgm^{-4}, which is larger than the density gradient by almost a factor of 5. This is in the order of π, and since the density anomaly of parcels convecting from the diffusive interface is $\sim\alpha\Delta T(\pi)^{-1}$ (section 4), they are buoyant enough to homogenise the initial intrusions.

External, lateral disturbances are likely to influence, and perhaps determine, the initial vertical scale of the interleaving. If the disturbances have high vertical wave numbers, or small vertical extent, the layers will be thin. The initial stability ratios are determined by the homogenisation of the vertical property gradients, and thin layers lead to stability ratios close to 1. The flux divergence could then cause the salt finger interface to overturn. Double-diffusive convection thus acts as a filter, which prevents too thin layers from surviving. Thicker layer with larger stability ratios will remain and evolve due to double-diffusive convection.

7   *Advection and expansion of the layers*

However, to create intrusions waters from the two sides of the front have to interleave, which requires that the vertical double-diffusive transport creates a pressure field that drives the water across the front. The flow across the front have been discussed by *Stern* (1967), *Toole and Giorgi* (1981), *Garrett* (1982), *McDougall* (1985a, b), *Ruddick* (1992). They all assume that the Coriolis acceleration is balanced by the along front slope of the layers, and that in the cross-front direction the force balance in a steady state is between the pressure gradients created by the buoyancy fluxes and the friction between the layers. The motion is thus assumed two-dimensional.

If the intrusions expand into the opposite water columns with constant velocity the property steps and the stability ratios at the interfaces are at each instant the same along the intrusion, even though the temperature and salinity vary. However, the reduction of the initial property steps by the double-diffusive transports is slower (by a factor ½) than in the rundown non-advective case discussed above because the expanding layers continuously bring water from the outside into the frontal zone.

The advection in the layers is due to the buoyancy force, which arises when the density of the layers changes relative to the density field of the undisturbed water column. The change in density F_Bh^{-1} caused by the double-diffusive fluxes triggers a displacement in the density field that acts to bring the parcel in equilibrium with its surroundings. This advection occurs with the velocity v and the angle ϕ relative to the isopycnals. This leads to;

$$\frac{F_B}{h} = vsin\varphi\rho_*^{-1}grad\rho \tag{23}$$

The buoyancy force is given by $g(\rho - \rho_o)sin\phi$, if the undisturbed isopycnals are horizontal and no external shear is present. The density perturbation $(\rho - \rho_o) = \delta\rho$, where ρ_o is the initial density, corresponds to a vertical distance in the stratification, and since two neighboring layers move in the opposite direction this gives a lower limit on the thickness of the layers;

$$\delta\rho \le 0.5hgrad\rho \tag{24}$$

To estimate the lateral velocities the along-layer buoyancy force and the retarding frictional drag must be assessed. Salt fingers exchange mass between the layers and this mass has to be accelerated, changing its velocity from –v to +v, as it passes from one layer to the other. No mass flux takes place through the diffusive interface, but plumes are injected from the same position at the interface into the layers above and below. This implies that there is an initial velocity difference between the layers and the convecting parcels (Fig. 11). Convection is triggered, both at the diffusive and at the salt finger interface, by heat conduction, and the mass needed to carry a comparable density anomaly into the layers must be of the same order for both interfaces. At the simpler diffusive interface the critical thickness of the unstable layer can be estimated to $\delta_c = (\pi\kappa_T t_c)^{1/2}$ with t_c being the critical time. Ignoring the diffusive transport of salt, the amount density anomaly diffusing through the interface during t_c is;

$$F_{\alpha T}^D t_c = \frac{\alpha\Delta T\delta_c}{\pi} \tag{25}$$

The mass transport into the layer per unit volume and time then becomes;

$$\dot{m} = \frac{\rho_*\delta_c}{t_c h} = \frac{\pi\rho_* F_{\alpha T}^D}{\alpha\Delta Th} \tag{26}$$

The mass flux across the interfaces can then be related to the corresponding transports of αT and βS as;

$$\dot{m} = \frac{\pi\rho_*(F_{\alpha T}+F_{\beta S})}{\alpha\Delta Th} = \frac{\pi\rho_* F_{\alpha T}}{\alpha\Delta Th}(1 + Rf^{-1}) \tag{27}$$

where $F_{\alpha T}$ and $F_{\beta S}$ are positive and includes the transports from both interfaces. The cross-front momentum balance can then be written as;

$$1.5v\dot{m} = g\delta\rho sin\varphi = \frac{1.5v\pi\rho_*(1+Rf^{-1})F_B}{\alpha\Delta Th(1-Rf^{-1})} \tag{28}$$

The factor 1.5 arises from the different velocity jumps at the two interfaces. Using equations 23 and 24 v is estimated to;

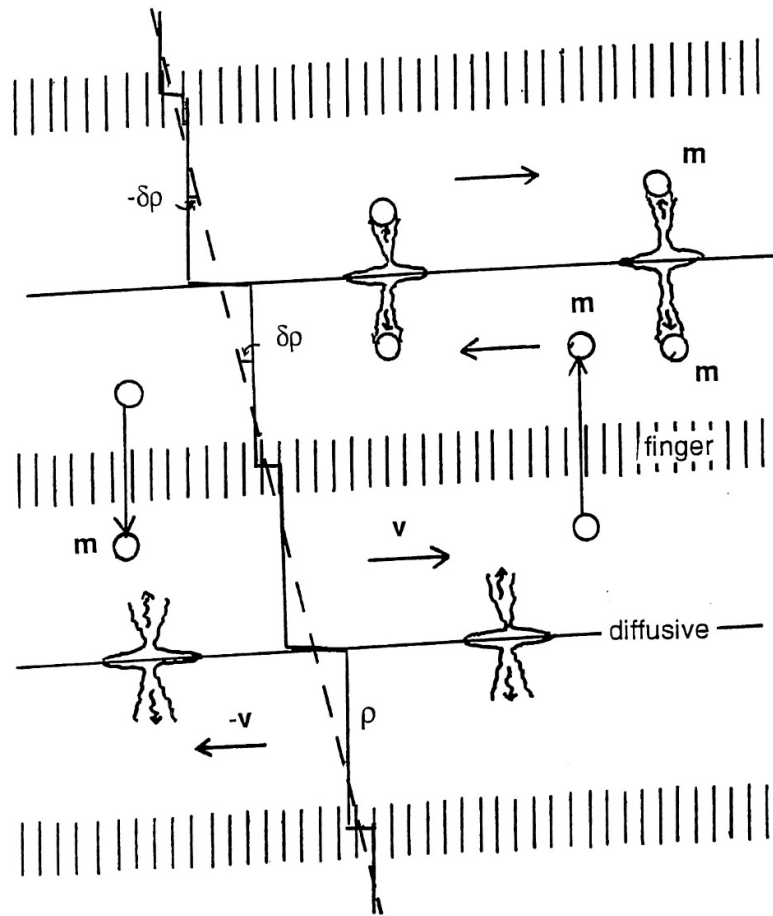$$v^2 \le \frac{g\alpha\Delta Th(1-Rf^{-1})}{3\pi(1+Rf^{-1})} \tag{29}$$

Fig. 11. Schematics showing the motions in the layers and the diffusive and salt finger convection and the change in the initial, linear density profile (broken line) into a step profile (solid line). The drawing assumes that the diffusive fluxes dominate. m is the mass convected from the diffusive interface and through the salt finger interface and v is the velocity in the layers.

For the low temperatures in the Arctic Ocean $\alpha = 0.8 \times 10^{-4}$ and $\beta = 8 \times 10^{-4}$ and with the use of $\Delta T = 0.5$ °C and $\Delta S = 0.05$ we have $\alpha \Delta T = \beta \Delta S = 4 \times 10^{-5}$. The velocity, the angle with the horizonal, and the penetration distance of the intrusions are shown in Fig. 12 as functions of time. The left panel gives the effects of different $R\rho$ and the right panel indicates the importance of property contrasts and layer thickness. The estimates are computed for the maximum velocity, with $\leq$ replaced by $=$, in Equation 29. The assumed thickness of the layers is 25 m, and with $R\rho=1.02$ the salt finger interface would rapidly overturn. For $R\rho=1.1$ the diffusive interface dominates the transports for a fairly long time, 250 hours, and with a mean velocity around 0.003 ms^{-1} the intrusions would by then penetrated almost 4000 m into the opposite water mass. The velocity in the layers decreased from ~0.01 ms^{-1} to zero from the initial small stability ratio to the change in sign of the buoyancy flux. Thereafter the salt finger transports are the largest. The computed velocity increases for a short period and then remains almost constant during the rest of the computation period (Fig. 12). The angle between the layers and the horizontal also

goes through zero indicating a change in sign of the slope as the salt finger flux starts to dominate. For Rρ > 1.5 the salt finger flux is the largest from the outset and the slope does not change sign.
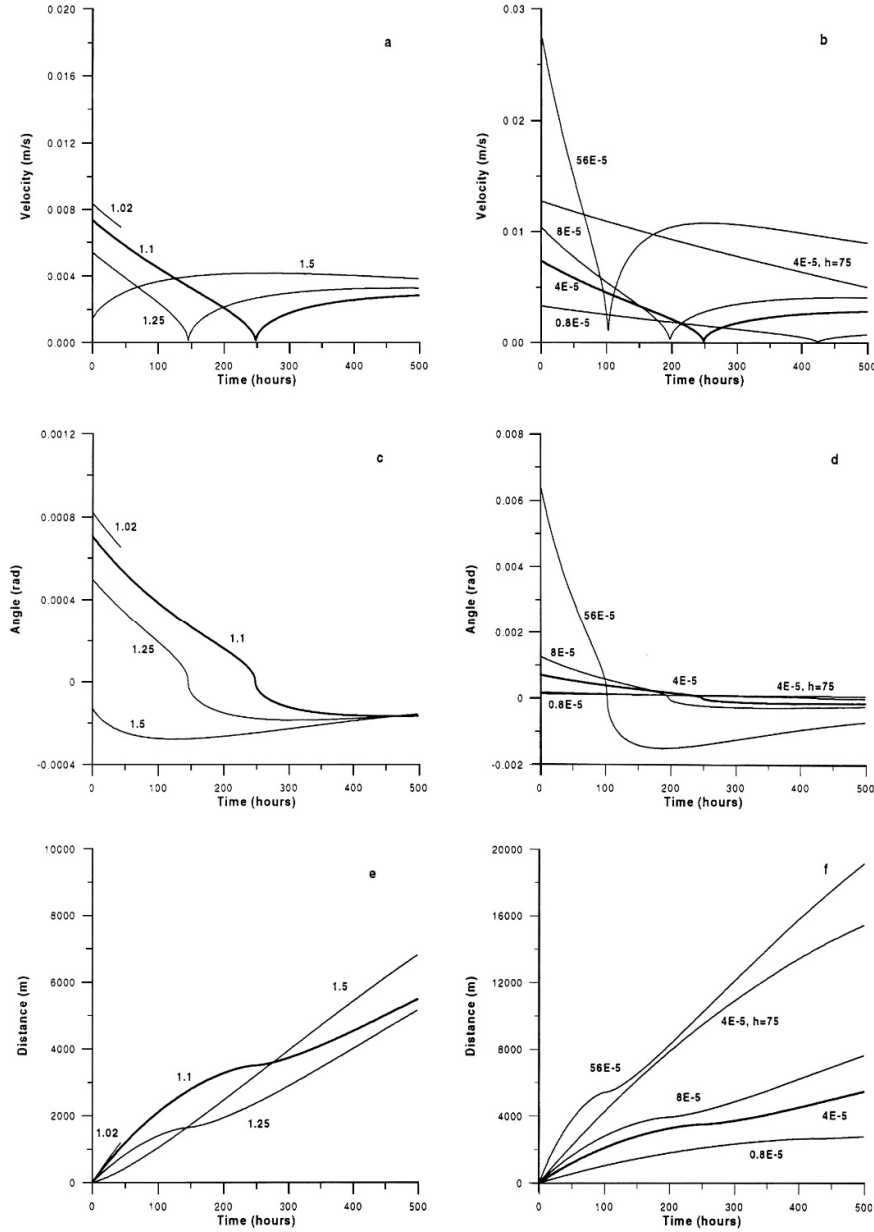

Fig. 12. The velocity in the layers (a & b), the slope of the layers relative to the horizontal (c & d) and the distance of penetration of the layers into the opposite water mass (e & f). The left panel gives the dependence on the initial stability ratio Rρ for the initial property steps $\alpha\Delta T_o=\beta\Delta S_o=4\times10^{-5}$. The right panel shows the effects of different initial property steps $\alpha\Delta T_o=\beta\Delta S_o$ for Rρ=1.1. and h=25m except when indicated otherwise.

As expected, larger property steps lead to large initial velocities and the highest computed velocity was about 0.03 ms^{-1} for $\alpha\Delta T_o = \beta\Delta S^o = 56\times10^{-5}$, but the velocity

decreased rapidly to zero and then increased to 0.01 ms^{-1} during the salt finger dominated phase. Smaller steps and also larger layer thickness cause the instant of zero velocity to occur later. The higher velocities found for the thicker layers are due to larger $\delta\rho$ with respect to the background stratification, and the assumption that the velocity is at its maximum may then be questionable. For the case with h=75m (Fig. 12) and the same initial density step the crossover point is reached after 1000 hours and the mean velocity is about 0.005 ms^{-1} and the penetration of the intrusions would be about 20 km. This corresponds to a width of the interleaving of 40 km and the thinner layers would have lateral extensions less than 10 km, provided that the spreading stops, when the salt finger fluxes become the largest. This is not as large as the observed extensions of the intrusions in the Arctic Ocean (*Rudels et al*., 1994; *Carmack et al*., 1997; *Carmack et al*., 1998; *Rudels et al*., 1999, see also Fig. 2).

For the interleaving to again expand after the change of sign in the buoyancy flux the entire layering structure must adjust its slope. The expansion is therefore likely to be arrested for a longer period during which the properties steps run down and the interfaces become less active. Only when Rρ is initially large or when the background stratification is unstable in the salt finger sense do the salt finger fluxes dominate from the outset and the layers can expand without the velocity going through zero and the slope changing sign. Large initial Rρ also implies large initial layer thicknesses and the observed Rρ^D at the diffusive interfaces should then be smaller than Rρ^F. This is not the case in the Arctic Ocean, where observations show that Rρ^D is almost always larger than Rρ^F, which indicates that in the initial phase the fluxes through the diffusive interface have been the strongest.

Here it may be appropriate to relate to the study by *Ruddick et al*. (1999), where they re-examine the *Ruddick and Turner* (1979) experiments. They find that in the central part of the interleaving the slopes of the intrusions are such that warm, saline intrusion rise and cold, fresh intrusions sink. This is in agreement with the salt finger interfaces transporting density anomalies more efficient than the diffusive interfaces. However, they also remark that the noses of the intrusions do not have this slope but are more or less horizontal (*Ruddick et al*., 1999, Fig. 14). Actually, when looking at the photographs from the experiments (e.g. *Ruddick and Turner*, 1979, Fig. 3) there appears to be a slight deflection of the nose from the horizontal in the sense that the warm intrusions sink, the cold intrusions rise, as would be the case, if the buoyancy fluxes through the diffusive interfaces are the strongest.

The noses represent the initial part of the intrusions. When the layers expand, the properties of the water change due to double-diffusive fluxes as it is advected in the layers. The stability ratio then increases, and when the water parcels have reached the position of the initial front, the salt finger fluxes might have become the largest, and the slope in the central part of the layering adjusts to this. However, at the noses the diffusive fluxes could still dominate and the slope of the layers becomes wavy. This is partly a support for the view that the buoyancy fluxes go through zero and that an initial, diffusively dominated, state changes into a salt finger dominated one.

It is interesting that on the salinity section shown in Fig. 2 it looks like the intrusions on the basin side of the salinity maximum display a similar wavy structure, the warm saline intrusions rise in the central part of the interleaving but are almost horizontal, or move slightly downwards at the edge of the interleaving, where the intrusions enter the colder Barents Sea branch water. This would be in agreement that the intrusions change slope and that they also could continue to expand after the salt finger transports have become the largest.

We have assumed that the velocity is constant and that the properties steps change at the same rate, keeping the stability ratio constant along the layers. The results shown by *Ruddick et al*. (1999) suggest that this may not the case. They found that the along layer velocities were not constant along the layers but were higher in the central part suggesting recirculation within the layers. Whether this is always true, or if it is due to the small layer thickness, which in the laboratory is of the same order as the salt finger length, or caused by the larger property steps used in the laboratory, or by the presence of vertical end walls, or due to the smaller difference between the diffusion coefficients we cannot tell. Leaving this question open, we continue to explore the consequences of constant velocities along the layers.

A further aspect is that advection in the layers implies an along-front slope as well as the cross-front slope of the layers because the flow across the front is geostrophically balanced by along-front slopes in the density surfaces (e.g. *Garrett*, 1982). For a cross front velocity of e.g. 0.005 m^{-1}, as suggested by *Carmack et al*. (1997) and *Swift et al*. (1997) for the layering observed in the Arctic Ocean, this corresponds, with a vertical density gradient of 0.4×10^{-3} kgm^{-4} and a layer thickness of 25 m, to an along-front slope 0.014 of the density surface using the thermal wind equation. This is much larger than the cross-front slope 0.0004 found here for the same velocity (Fig. 12).

Since the flow changes direction between the layers the along-front slope of the density surface must vary to create the pressure gradients needed to balance flows in both direction, and the slope of the layers must be still larger (Fig. 13). The vertical change in density is largest at the interface that has the highest transport of density anomaly, in Figure 13 indicated by closer spacing of the density surfaces. The density must increase to the right of the flow direction and this lead also to a different along-front slope of the layer, depending upon if the diffusive or the salt finger interfaces are most effective.

For the observed large extension of the intrusions in the Eurasian Basin the change of depth of the layers across the front would be >100m and more than the depth of the basins in the along-front direction. The observed cross-front depth change of the layers is less than this (Fig. 2). Large depth changes are also not seen along the front, but it is possible, but perhaps not probable, that the layering structure consists of several sloping sheets, starting at the bottom of the layering and disappearing at the top (Fig. 13). This argues against a direct spreading, driven by double-diffusive convection, of the intrusions from the continental slope into the basin. A perhaps more reasonable explanation would be that the intrusions are advected with the mean flow and, as a part of the boundary current, detach from the continental slope and enter the Eurasian Basin north of the Laptev Sea (*Rudels et al*., 1994).
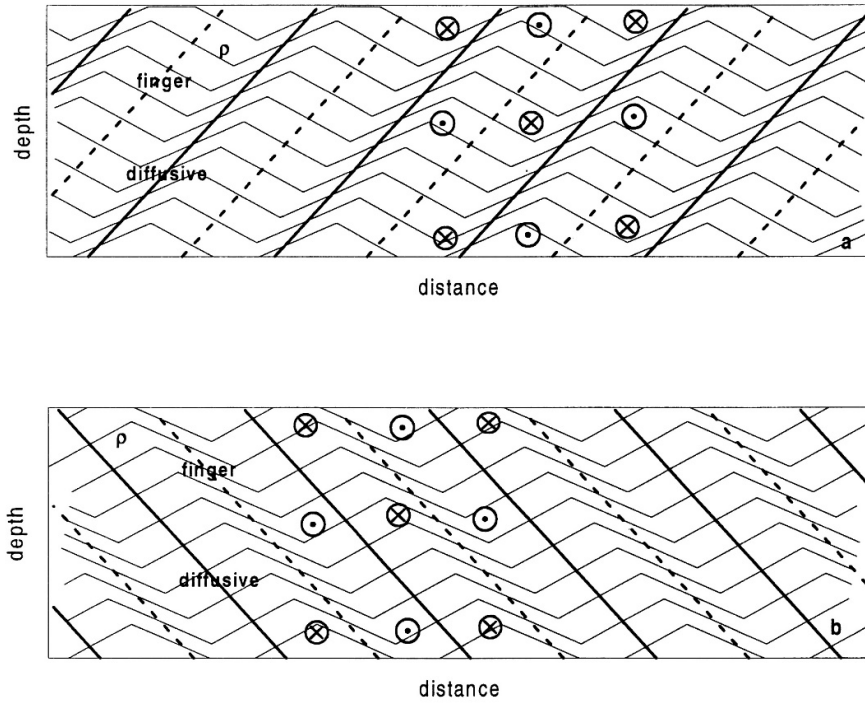
Fig. 13. The along-front situation of a layering structure. The thin lines indicate isopycnals and bold, solid lines diffusive interfaces, bold, broken lines salt finger interfaces. Warm intrusions move out of the plane, and the velocity is taken to be zero at the interfaces. a) The heat transport dominates, the stability at the diffusive interface increases most rapidly, and warm intrusions become denser. b) The salt transport dominates, the stability at the salt finger interface increases the most and warm intrusions become less dense. The sense of the along-front slope of the layers is different in the two situations.
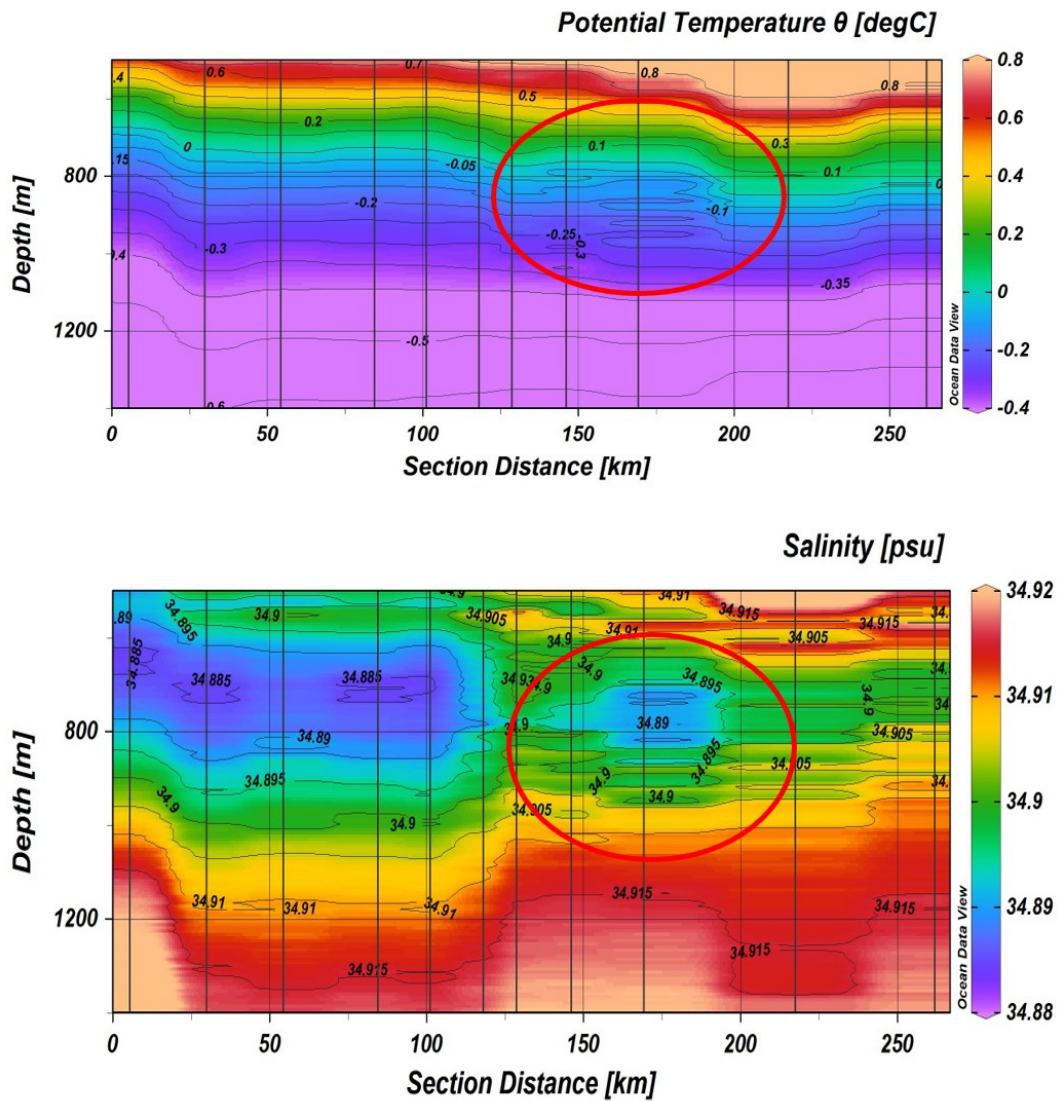
Fig. 14a. Potential temperature (upper panel) and salinity (lower panel) sections in the Nansen Basin taken in 1996 revealing a deep cold, and less saline eddy of Barents Sea branch water (red ellipses) separated from the main core of the Barents Sea inflow farther into the basin. The diameter of the eddy is about 75 km and the intrusions at the rim of the eddy extend about 20 km, more than twice the estimated spreading of the intrusions (Fig. 12).
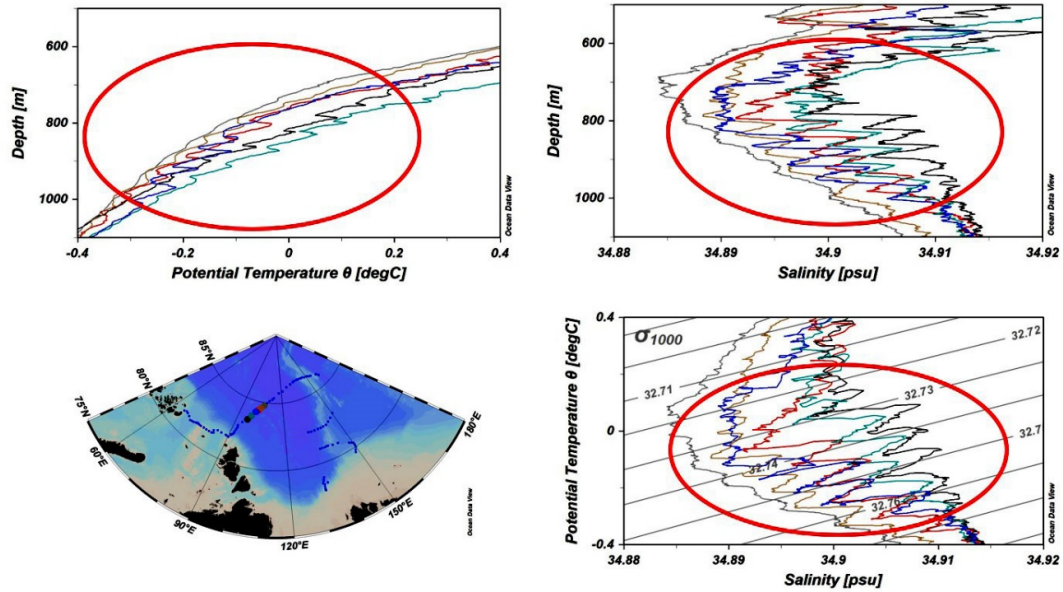
Fig. 14b. Potential temperature and salinity profiles and TS curves from stations taken through the eddy (red ellipses). The section and the station positions are shown on the map. The eddy is located in the depth range where the background stratification is stable in both temperature and salinity.

8   Summary

The possibility of creating inversions and double-diffusively driven intrusions at the front between the two Atlantic inflows to the Arctic Ocean, the Fram Strait branch and the Barents Sea branch, as they converge on the Kara Sea slope has been discussed. Different stratifications are considered and an idealized approach is applied, where the horizontal difference in temperature between the two water columns together with the salinity and temperature stratifications determine the maximum thickness of the created intrusions. Except when temperature is unstably stratified the derived thicknesses are larger than observed, which suggests that the vertical scale might be set by external disturbances that generate the initial inversions. If an intrusion penetrates across the front as in a lock-exchange flow the vertical scale of one single disturbance may spread to the compensating return flows above and below.

Laboratory and theoretically derived $(\alpha\Delta T)^{4/3}$ and $(\beta\Delta S)^{4/3}$ flux laws are applied at the diffusive and salt finger interfaces, and the changes in the properties of the intrusions with time and their expansion into the opposite water mass are estimated for the case where both salt and heat are stably stratified and their contributions to the vertical density increase are equal. With the applied flux laws the transport through the diffusive interface is initially the largest and cold, fresh intrusions rise and warm saline intrusions sink, and for small initial stability ratios the salt finger interface might overturn but for larger $R\rho$ the interfaces remain stable. Since the $R\rho^D$ at the diffusive interface increases more rapidly than $R\rho^F$, the fluxes through the salt finger interfaces eventually dominate. The cross-front slope would then change and the warm saline intrusions begin to rise and the cold fresh intrusions to sink. This implies that the entire interleaving structure would flip over,

which appears unlikely, and the interpretation favoured here is that the spreading of the intrusions then essentially stops, and they are carried as fossil intrusions by the mean circulation, which explains their spreading and observed large extent in the Arctic Ocean basins.

For intrusive layers 25 m thick the initial velocity is slightly less than 0.01 ms^{-1} and they would expand for about 200 hours before the velocity has decreased (almost linearly) to zero. The distance the intrusions have spread ranges between 2000 m to 4000 m, creating interleaving structures between 4000 m to 8000 m wide. This presumes no further expansion, when the salt finger fluxes start to dominate. This estimates naturally depend on the chosen flux laws but should be reasonable, if the underlying approach is valid.

The changes in the vertical double-diffusive transports given here are only due to the increase of Rρ with time, and the effects of different property steps have not been considered. The initial property steps depend upon the stratification as seen from the slopes of the TS curves (Fig. 5). The strongest effect is present when the temperature is unstably stratified (Figs 4 & 5). Then $\alpha\Delta T_o$ is much larger than $\beta\Delta S_F$ and the difference in fluxes is mainly due to the magnitude of the property steps and not on the flux law dependence on Rρ. This implies that the transports through the diffusive interfaces are much larger than those through the salt finger interfaces, and intrusions formed in the part of the water column where temperature is unstably stratified the salt finger interfaces are likely to overturn. The intrusions would then be transformed into thermohaline staircases with thick homogenous layers. Such thick layers have been reported from north of Severnaya Zemlya and the Laptev Sea (*Polyakov et al.*,2019). This topic will not be pursued any further here.

The confluence of the two inflow branches not only leads to interleaving but also to the formation of eddies comprised of either Fram Strait branch water or Barents Sea branch water. One cold, less saline eddy of Barents Sea branch water was observed in 1996 in the Nansen Basin, separated from the main Barents Sea branch farther into the basin (Fig. 14). The life time and rundown of eddies has been discussed by *Ruddick and Hebert* (1988) in the case of a warm, saline Mediterranean eddy and by *Bebieva and Timmermans* (2016) considering a warm, saline eddy in the Canada Basin. There are three possibilities for the warm eddy to rundown, diffusive fluxes vertically upwards in the upper part, salt finger fluxes downward in the lower part, and lateral exchanges by thermohaline intrusions. *Ruddick and Hebert* (1988) focused on the intrusions and estimated the extent of the interleaving zone to 15 km and the velocity to 0.001 ms^{-1}. *Bebieva and Timmermans* (2017) considered the salt finger fluxes to be the most efficient mechanism to remove the anomalous water of the eddy but assumed that intrusions might also contribute significantly.

In the Nansen Basin the water column was stably stratified in both temperature and salinity and several intrusions were present at the front between the eddy and the ambient water. Are these intrusions still active and do they contribute to the disappearance of the eddy? Even if the intrusions have expanded far and are close to the passive state the relative motion between the ambient water and the eddy could rip off the outer part of the cold intrusions and allow ambient water to be drawn into the interleaving structure. This

would induce a compensating outflow of cold water from the eddy, which would gradually disappear. The radius of the eddy was around 50 km and the extension of the intrusions appeared to be between 10 km and 15 km (Fig. 14). If the water in the intrusions advects with a velocity of 0.001 ms^{-1} it would take about a year for an intrusion of ambient water to reach the centre of the eddy. This is probably too high a velocity, if the interleaving is close to rundown and the survival time of the eddy is probably longer.

Acknowledgements

References

Bebieva, Y. and M.-L. Timmermans, 2016. An examination of double-diffusive processes in a meso-scale eddy in the Arctic Ocean, *J. Geophys. Res.*, **121**, 457–475.

Bebieva, Y. and M.-L. Timmermans, 2017. The relationship between double-diffusive intrusions and staircases in the Arctic Ocean, *J. Phys. Oceanogr.*, **47**, 867–878.

Benjamin, T.B., 1968. Gravity currents and related phenomena. *J. Fluid Mech.*, **31**, 209–248.

Carmack, E.C., K. Aagaard, J.H. Swift, R.W. Macdonald, F.A. McLaughlin, E.P. Jones, R.G. Perkin, J.N. Smith, K.M. Ellis and L.R. Killius, 1997: Changes in temperature and tracer distributions within the Arctic Ocean: Results from the 1994 Arctic Ocean section, *Deep-Sea Research II*, **44**, 1487–1502.

Carmack, E.C., K. Aagaard, J.H. Swift, R.G. Perkin, F.A. McLaughlin, R.W. Macdonald and E.P. Jones, 1998. Thermohaline transitions. In "*Physical Processes in Lakes and Oceans*" Ed. J. Imberger, Coastal and Estuarine Studies **54**, American Geophysical Union, Washington, DC, 179–186.

Crank, J., 1956. The mathematics of diffusion, Oxford, Clarendon Press, 347 pp.

Foldvik, A and B. Rudels, 1996. Double-diffusive Experiments. In "*Waves and non-linear Processes in Hydrodynamics*" Eds. B. Gjevik, J. Grue and J.E. Weber, Kluwer Acad. Publ., Dordrecht, 239–254.

Garrett, C., 1982. On the parameterisation of diapycnal fluxes due to double-diffusive intrusions. J. *Phys. Oceanogr.*, **12**, 952–959.

Holyer, J.A., T.J. Jones, M.G. Priestly and N.C. Williams, 1987. The effect of vertical temperature and salinity gradients on double-diffusive interleaving. *Deep-Sea Res.*, **34**, 517–530.

Howard, L.N., 1967. Convection at high Rayleigh number. In "*Proc. eleventh Congress Applied Mech., München*", Ed. H. Görtler, Springer Verlag, Berlin, 1109–1115.

Kelley, D.E. 1984. Effective diffusivities within oceanic thermohaline staircases. *J. Geophys. Res.*, **89**, 10449–10488.

Kelley, D.E. 1990. Fluxes through diffusive interfaces: A new formulation. *J. Geophys Res.*, **95**, 3365–3371.

Kelley, D. E., H.J.S. Fernando, A.E. Gargett, J. Tanny and E. Ozsoy, 2003. The diffusive regime of double-diffusive convection. Progress in Oceanography, 56, 461–481.

Kunze, E., 1987. Limits of growing finite-length salt fingers. A Richardson number constraint. *J. Mar. Res.*, **45**, 533–556.

Kuzmina, N., B. Rudels, V. Zhurbas and T. Stipa, 2011. On the structure and dynamical features of intrusive layering in the Eurasian Basin of the Arctic Ocean. *J. Geophys. Res.*, **116**, C00D112.

Linden, P.F. and T.G.L. Shirtcliffe, 1978. The diffusive interface in double-diffusive convection. *J. Fluid Mech.,* **87**, 417–432.

May, B.D. and D.E. Kelley, 1997. Effect of baroclinicity on double-diffusive interleaving. *J. Phys. Oceanogr.*, **27**, 1997–2008.

May, B.D. and D.E. Kelley, 2002. Growth and steady stages of thermohaline intrusions in the Arctic Ocean. *J. Geophys. Res.*, **106**, 16783–16794.

McDougall, T.J., 1985a. Double-diffusive interleaving Part I: Linear stability analysis. *J Phys. Oceanogr.*, **15**, 1532–1541.

McDougall, T.J., 1985b. Double-diffusive interleaving Part II: Finite amplitude steady state interleaving. *J Phys. Oceanogr.*, **15**, 1542–1556.

McDougall, T.J., 1986. Oceanic intrusions: some limitation of the Ruddick and Turner (1979) mechanism. *Deep-Sea Res.*, **33**, 1653–1664.

Merryfield, W.J. 2002. Intrusions in double-diffusivly stable Arctic waters: Evidence for differential mixing?. *J. Phys. Oceanogr.*, **32**, 1452–1459.

Perkin, R.G., and E.L. Lewis, 1984. Mixing in the West Spitsbergen Current, *J. Phys. Oceanogr.*, **14***, 1315–1325.

Polyakov, I.V., L. Padman, Y.-D Lenn, A.V. Pnyushkov, R. Rember and V.V. Ivanov, 2019. Eastern Arctic Ocean diapycxnal heat flux through large double-diffusive steps. *J Phys. Oceanogr.*, **49**, 227–246.

Quadfasel, D., A. Sy, and B. Rudels, 1993. A ship of opportunity section to the North Pole: Upper ocean temperature observations. *Deep-Sea Res.*, **40**, 777–789.

Radko, T. 2013. Double-Diffusive Convection. Cambridge Univ. Press, 342 pp.

Rippeth, T.P., B.J. Lincoln, Y.-D. Lenn, J.M. Green, A. Sundfjord and S. Bacon, 2015. Tide-mediated warming of Arctic halocline heat fluxes over rough topography. *Nature Geosci.*, **8**, 191–194.

Ruddick, B., 1984. The life of a thermohaline intrusion. *J. Mar. Res.*, **42**, 831–852.

Ruddick, B., 1992. Intrusive mixing in a Mediterranean salt lens: intrusion slopes and dynamical mechanisms. *J. Phys. Oceangr.*, **22**, 1274–1285.

Ruddick, B. and J.S. Turner, 1979. The vertical scale of double-diffusive intrusions. *Deep-Sea Res.*, **26**, 903–913.

Ruddick, B. and D. Hebert, 1988. The mixing of meddy "Sharon". In "*Small-scale mixing and turbulence in the ocean*". Eds. J.C.N. Nihoul and B.M. Jamart Elsevier, Amsterdam, 481–502.

Ruddick, B, O.M. Phillips and J.S. Turner, 1999. A laboratory and quantitative model of finite amplitude thermohaline intrusions. *Dyn. Atmos. and Ocean*, **30**, 71–99.

Rudels, B., E.P. Jones, L.G. Anderson and G. Kattner, 1994. On the intermediate depth waters of the Arctic Ocean. In "*The role of the Polar Oceans in Shaping the Global Climate.*" Eds. O.M. Johannessen, R.D. Muench and J.E. Overland, American Geophysical Union, Washington D.C., 33–46.

Rudels, B., G. Björk, R.D. Muench and U. Schauer, 1999. Double-diffusive layering in the Eurasian Basin of the Arctic Ocean. *J. Mar. Systems,* **21**, 3–27.

Schlitzer, R, 2017. Ocean Data View. http//odv.awi.de

Stern, M.E., 1960. The "salt fountain" and thermohaline convection. *Tellus*, **12**, 172–175.

Stern, M.E., 1967. Lateral mixing of water masses. *Deep-Sea Res.*, **14**, 747–753.

Swift, J.H., E.P. Jones, E.C. Carmack, M. Hingston, R.W. Macdonald, F.A. McLaughlin and R.G. Perkin, 1997. Waters of the Makarov and Canada Basins. *Deep-Sea Res. II*, **44**, 1503–1529.

Toole, J.M. and D.T. Georgi, 1981. On the dynamics and effects of double-diffusively driven intrusions. *Prog. in Oceanogr.*, **10**, 121–145.

Turner, J.S., 1965. The coupled turbulent transports of salt and heat across a sharp density interface. Int. J. Heat and Mass Trans., **8**, 759–767.

Turner, J.S., 1967. Salt fingers across a density interface. *Deep-Sea Res*., **14**, 599–611.

Turner, J. S., 1973: Buoyancy Effects in Fluids. Cambridge Univ. Press, Cambridge, 367pp.

Veronis, G., 1965. On finite amplitude instability in thermohaline convection. J. Mar. Res., **23**, 1–17.

Veronis, G., 1968. Effect of a stabilizing gradient of solute on thermal convection. *J. Fluid Mech*., **34**, 3215–336.

Walsh, D and E.C. Carmack, 2002. A note on evanescent behaviour of Arctic thermohaline intrusions. *J Mar. Res.*, **60**, 281–310.

Walsh, D. and E.C. Carmack, 2003. The nested structure of Arctic thermohaline intrusions. *Ocean Mod.*, **5**, 267–289.